

Saddle-splay term induced orientational instability in nematic liquid crystal cells and director fluctuations at substrates

A.D. Kiselev^{1,*}

¹*Chernigov State Technological University,
Shevchenko Street 95, 14027 Chernigov, Ukraine*

(Dated: September 18, 2018)

Abstract

We analyze stability of the planar orientational structure in a nematic liquid crystal (NLC) cell with planar anchoring conditions at both substrates. Specifically, we study the instabilities of the ground state caused by surface elasticity at large saddle-splay elastic constant, K_{24} . We show that such instabilities are induced by the director fluctuations at confining walls and derive the surface part of static correlation functions as a functional integral over these fluctuations characterized by the surface free energy. From the surface part of the correlator we derive the stability conditions for the planar structure with respect to the fluctuation modes characterized by the in-plane wavenumbers and by the parity symmetry. These conditions are analyzed in the cell thickness – fluctuation wavelength plane by using the parameterization for the boundary curve of the instability region. For relatively small K_{24} violating the Ericksen inequalities $0 < K_{24} < 2 \min(K_1, K_2)$ the theory predicts that the critical fluctuation mode of the wavelength, λ_c , will render the structure unstable when the thickness of the cell is below its critical value, d_c . The parity of the critical mode changes as the twist-splay ratio K_2/K_1 is passing through the unity. Further increase of K_{24} beyond the second threshold value, $4K_1K_2/(K_1 + K_2)$, leads to the instability with respect to the short wavelength fluctuations regardless of the cell thickness. We compute the critical thickness and the critical wavelength as functions of K_{24} , the twist-splay ratio and the azimuthal anchoring strength.

PACS numbers: 61.30.Gd, 64.70.Md, 61.30.Hn

I. INTRODUCTION

Nematic liquid crystals (NLC) confined in restricted geometries are technologically important [1] and have been the subject of intense studies over the past few decades [2, 3]. Anisotropy of the vast majority of NLCs is locally uniaxial and molecules of a NLC align on average along a local unit director. Orientational structures in NLCs are thus defined by distributions of the director $\mathbf{n}(\mathbf{r})$ and the well-established continuum elastic theory provides the phenomenological description of orientational distortions [4, 5].

In the absence of external fields, orienta-

tional structures in spatially bounded NLCs crucially depend on the conditions at confining walls. These are macroscopically characterized by the surface contribution to the elastic free energy, F_s , that adds to the Frank elastic energy, F_b , describing elasticity of NLC in the bulk, to yield the total elastic free energy of a NLC in the presence of the confining surfaces

$$F[\mathbf{n}] = F_b[\mathbf{n}] + F_s[\mathbf{n}], \quad (1)$$

$$F_b = \frac{1}{2} \int_V \left[K_1 (\nabla, \mathbf{n})^2 + K_2 (\mathbf{n}, \nabla \times \mathbf{n})^2 + K_3 [\mathbf{n} \times (\nabla \times \mathbf{n})]^2 \right] dv, \quad (2)$$

*Email address: kisel@elit.chernigov.ua

$$F_s = \frac{1}{2} \int_S \left[W(\mathbf{n}) - K_{24} [(\boldsymbol{\nu}, \mathbf{n})(\nabla, \mathbf{n}) - (\boldsymbol{\nu}, (\mathbf{n}, \nabla)\mathbf{n})] \right] ds, \quad (3)$$

where K_1 , K_2 and K_3 are the splay, twist and bend elastic constants, respectively; K_{24} is the saddle-splay elastic constant; $\boldsymbol{\nu}$ is the outer normal to the surface S ; $W(\mathbf{n})$ is the surface density of the anchoring energy.

An important point is that, in addition to the anchoring energy which is the anisotropic part of the surface tension, there is also the elastic contribution to the surface free energy that, originally, has been indicated as a part of the elastic energy having the form of a divergence [6, 7, 8]. This contribution — the so-called saddle-splay term (the K_{24} term) — can generally be viewed as the tangential director gradient dependent elastic part of the surface energy [9, 10]. The other surface elastic term known as the K_{13} term will not be considered in this paper as it can be ignored in cases where spatial variations of the density and the scalar order parameter are of minor importance [11, 12, 13].

In the last years K_{24} specific issues have attracted much less attention than the fundamental difficulties caused by the K_{13} term. In particular, though the exact measurements of K_{24} are still missing it was experimentally estimated to be of the order of the Frank elastic constants [14, 15, 16]. One of the most important theoretical results is that the K_{24} term may induce spontaneous twist deformations in hybrid nematic films with azimuthally degenerate anchoring conditions [17]. Such deformations are manifested in the formation of periodic stripe domains observed in sufficiently thin hybrid NLC cells [18, 19, 20].

For planar NLC cells, similar instability of the ground state in the presence of the K_{24} term was considered in Refs. [21, 22]. Recently, in Ref. [23], Barbero and Pergamenschik suggested that in the proximity of the nematic-smectic- A transition the K_{24} term grows anomalously large so as to violate

the Ericksen stability conditions [24]:

$$0 < K_{24} < 2 \min(K_1, K_2). \quad (4)$$

As a result, the uniform equilibrium director distribution becomes unstable and a periodically modulated nematic phase may occur in sufficiently thin planar films.

The results of Refs. [22, 23, 25] are essentially limited to the special case in which the azimuthal anchoring strength is identically zero. But the study of possible mechanisms leading to the formation of modulated orientational structures close to the nematic-smectic- A transition requires a quantitatively accurate description of the instability that goes beyond this limitation. At this stage, however, even the instability scenario as a whole has not been studied in any detail.

In this paper we intend to fill the gap. Our primary goal is the comprehensive study of the instability induced by the K_{24} term in the presence of the azimuthal anchoring.

The idea underlying our general theoretical considerations is that instabilities of this sort occur when the director fluctuations at confining surfaces become critically divergent. So, we suggest the method connecting the correlation functions of director fluctuations and the computational procedure applied to perform the stability analysis. This method is based on separating out the surface part of the correlator as a correlation function of the fluctuation field induced by the director fluctuations at confining walls.

The layout of the paper is as follows. In Sec. II, we express the surface part of the static correlation functions of the director fluctuations as a functional integral over fluctuations at confining walls and explicitly relate the procedure for computing the correlators to the stability conditions used in our stability analysis.

Analytical results for the planar NLC cell are described in Sec. III. We characterize the mirror symmetry properties of the fluctuation harmonics and calculate the surface part of the correlator. We find that the result is a

sum of the contributions from the two fluctuation modes of different symmetry (symmetric and antisymmetric) and derive the stability conditions for these modes.

Stability of the uniform planar orientational structure is studied in Sec. IV. We analyze the parameterization of the boundary curve enclosing the instability region in the thickness–wavelength plane and show that, in addition to the stability interval (4), there are two different intervals for K_{24} : (a) $2 \min(K_1, K_2) < K_{24} < 4K_1K_2/(K_1 + K_2)$, where the critical point is characterized by the critical thickness d_c and the critical fluctuation wavelength λ_c ; (b) $K_{24} > 4K_1K_2/(K_1 + K_2)$, where NLC cells of any thickness are unstable with respect to the short wavelength fluctuations with $\lambda < \lambda_\infty$. It is found that the critical fluctuation mode is antisymmetric at $K_2 < K_1$ and is symmetric at $K_2 > K_1$. The critical thickness and the critical wavelength are computed as functions of K_{24} and the azimuthal anchoring strength. We also discuss the spectrum of director fluctuations at the substrates near the critical thickness.

Finally, in Sec. V, we present our results and make some concluding remarks. Details on some technical results are relegated to Appendixes A and B.

II. CORRELATION FUNCTIONS AND STABILITY CRITERIA

In this section we consider the general procedure for computing the correlation functions (correlators) of NLC director fluctuations in confined geometry. We remind the reader about the standard approach that uses functional integrals to represent averaging over fluctuations [5, 26]. In this approach the effect of the confining surface enters the theory through the boundary conditions for the saddle point equations (Euler-Lagrange equations) and for the Green functions.

We then describe an alternative procedure, where the part of the fluctuation field

representing the director fluctuations at the surface is separated out by shifting the integration variable in the functional integral. The corresponding part of the correlator is defined by the surface part of the free energy (3) and involves averaging over the fluctuations at the surface. Finally, we show that the free energy of these fluctuations determines stability of orientational structures.

A. Free energy of fluctuations

Assuming that the director field \mathbf{n}_0 defines the unperturbed orientational structure, we shall write the distorted configuration in the form

$$\begin{aligned} \mathbf{n} &= \cos \theta \cos \phi \mathbf{n}_0 + \cos \theta \sin \phi \mathbf{n}_1 \\ &+ \sin \theta \mathbf{n}_2, \quad (\mathbf{n}_i, \mathbf{n}_j) = \delta_{ij}, \end{aligned} \quad (5)$$

where the brackets denote the scalar product. Locally, the vectors \mathbf{n}_0 and \mathbf{n}_1 form the \mathbf{n}_0 – \mathbf{n}_1 plane, so that the angles ϕ and θ describe in-plane and out-of-plane orientational distortions, respectively.

Substituting Eq. (5) into Eqs. (1) – (3) will give the free energy of the director configuration (5) as a functional of the angles ϕ and θ . For small distortions, $\phi, \theta \ll 1$, Eq. (5) reduces to the familiar form

$$\mathbf{n} \approx \mathbf{n}_0 + \delta \mathbf{n}_0, \quad \delta \mathbf{n}_0 = \phi \mathbf{n}_1 + \theta \mathbf{n}_2 \quad (6)$$

and the lowest order approximation for the free energy of director fluctuations — the so-called Gaussian approximation — is given by the second order term, $F^{(2)}$, of the truncated series expansion for the energy (1)

$$F[\mathbf{n}] \approx F[\mathbf{n}_0] + F^{(2)}[\boldsymbol{\psi}], \quad (7)$$

$$F^{(2)}[\boldsymbol{\psi}] = F_b^{(2)}[\boldsymbol{\psi}] + F_s^{(2)}[\boldsymbol{\psi}], \quad (8)$$

where $\boldsymbol{\psi} \equiv \begin{pmatrix} \psi_1 \\ \psi_2 \end{pmatrix} = \begin{pmatrix} \phi \\ \theta \end{pmatrix}$ is the two-component fluctuation field; $F_b^{(2)}$ and $F_s^{(2)}$ are the bulk and the surface parts of the fluctuation free energy generated by the corresponding terms of the free energy (1).

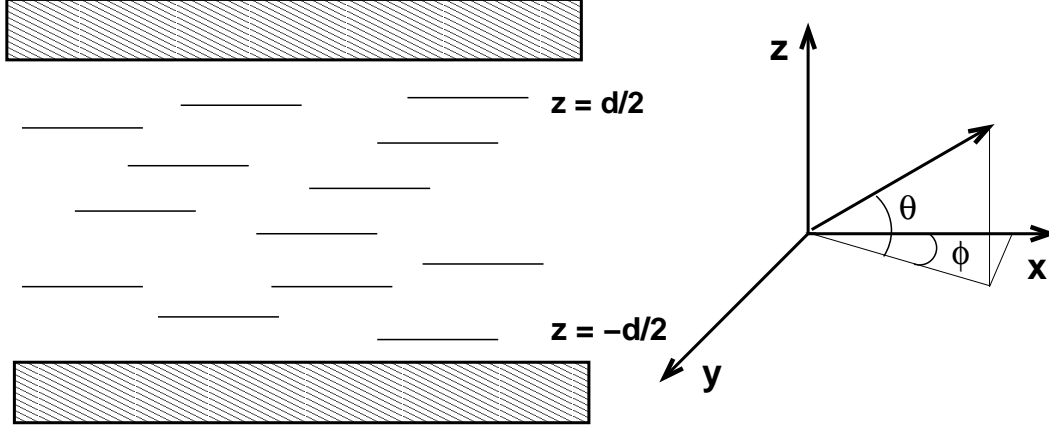


FIG. 1: Schematic representation of the planar NLC cell. In-plane and out-of-plane fluctuations are described by the angles ϕ and θ , respectively.

We can now apply the standard variational procedure to obtain the saddle point equations for the fluctuation free energy. (These equations can also be derived as the linearized Euler-Lagrange equations for the director (5)). In this section, we only need to specify the general form of the equations:

$$\frac{\delta F_b^{(2)}[\boldsymbol{\psi}]}{\delta \psi_i(\mathbf{r})} = \hat{K}_{ij} \psi_j(\mathbf{r}) \equiv [\hat{K} \boldsymbol{\psi}(\mathbf{r})]_i = 0, \quad (9)$$

where \hat{K} is the matrix differential operator. Hereafter, matrices and matrix differential operators will be indicated by hats and we also assume the summation over repeated indices.

The general structure of the fluctuation free energy can now be expressed as follows

$$F_b^{(2)}[\boldsymbol{\psi}] = \int_V (\boldsymbol{\psi}, \hat{K} \boldsymbol{\psi}) dv + \int_S (\boldsymbol{\psi}, \hat{Q}^{(b)} \boldsymbol{\psi}) ds, \quad (10)$$

$$F_s^{(2)}[\boldsymbol{\psi}] = \int_S (\boldsymbol{\psi}, \hat{Q}^{(s)} \boldsymbol{\psi}) ds. \quad (11)$$

where $(\boldsymbol{\varphi}, \hat{A} \boldsymbol{\psi}) \equiv \varphi_i \hat{A}_{ij} \psi_j$ and the surface term on the right hand side of Eq. (10) results from the integration by parts.

There are two most important formal properties of $F_s^{(2)}$ and $F_b^{(2)}$: (a) director derivatives along the normal to the surface do not enter $F_s^{(2)}$; and (b) the bulk free energy

$F_b^{(2)}$ is represented by the symmetric bilinear functional S_b , so that $F_b^{(2)}[\boldsymbol{\psi}] = S_b[\boldsymbol{\psi}, \boldsymbol{\psi}]$ and $S_b[\boldsymbol{\varphi}, \boldsymbol{\psi}] = S_b[\boldsymbol{\psi}, \boldsymbol{\varphi}]$. In particular, the relation

$$\begin{aligned} & \int_V [(\boldsymbol{\varphi}, \hat{K} \boldsymbol{\psi}) - (\boldsymbol{\psi}, \hat{K} \boldsymbol{\varphi})] dv \\ &= \int_S [(\boldsymbol{\psi}, \hat{Q}^{(b)} \boldsymbol{\varphi}) - (\boldsymbol{\varphi}, \hat{Q}^{(b)} \boldsymbol{\psi})] ds, \end{aligned} \quad (12)$$

which is a version of the Green formula, immediately follows from the symmetry of S_b .

B. Correlators and Green functions

We shall need to write the probability distribution of fluctuations at the state of thermal equilibrium in the form

$$P[\boldsymbol{\psi}] = Z^{-1} \exp\{-\beta F^{(2)}[\boldsymbol{\psi}]\}, \quad (13)$$

where $\beta \equiv (k_B T)^{-1}$, k_B is the Boltzmann constant, T is the temperature and Z is the partition function given by the functional integral

$$Z = \int \exp\{-\beta F^{(2)}[\boldsymbol{\psi}]\} \mathcal{D}\boldsymbol{\psi}, \quad (14)$$

where $\mathcal{D}\boldsymbol{\psi} \equiv \mathcal{D}\psi_1 \mathcal{D}\psi_2$. The components of the correlator then be written as the averages

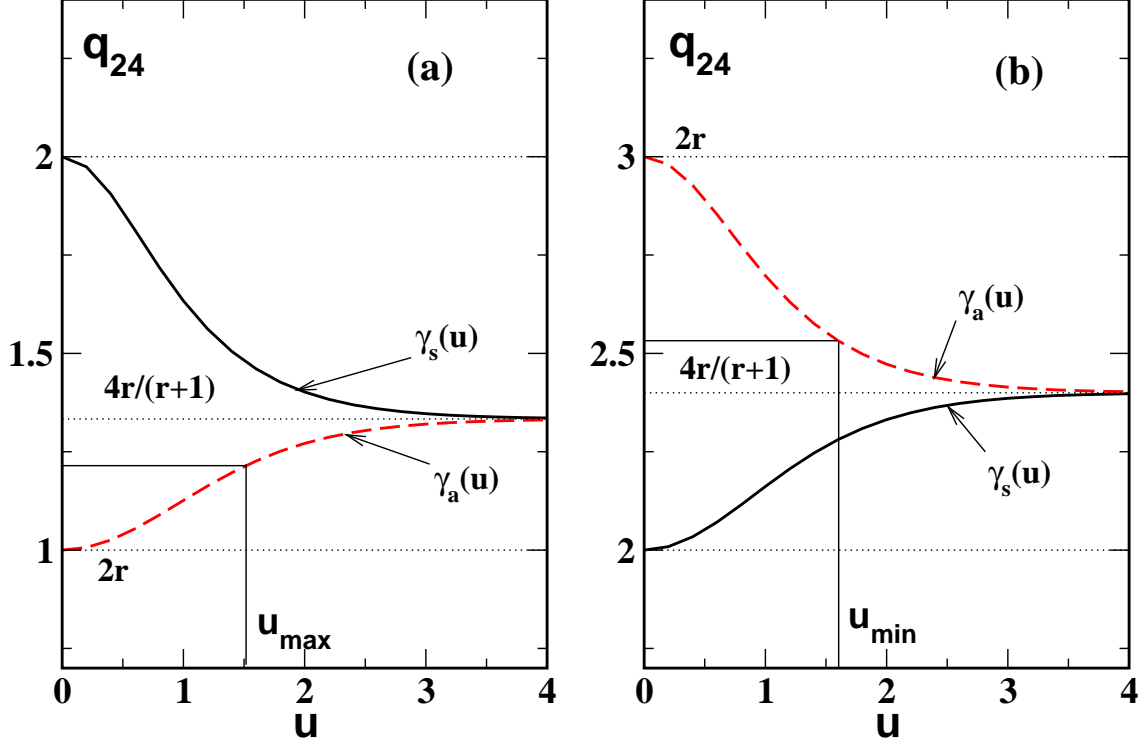


FIG. 2: The graphs of the functions $\gamma_s(u)$ (solid line) and $\gamma_a(u)$ (dashed line) in the u - q_{24} plane. Two cases are illustrated: (a) $r < 1$ ($r = 0.5$) and (b) $r > 1$ ($r = 1.5$). The endpoint of the instability interval for the critical mode $u < u_{\max}$ at $q_c^{(1)} < q_{24} < q_c^{(2)}$ is shown on the left. At $q_c^{(2)} < q_{24} < q_c^{(3)}$, the endpoint of the instability interval for the non-critical mode $u > u_{\min}$ is indicated on the right.

of the fluctuation field products

$$\begin{aligned} C_{ij}(\mathbf{r}, \mathbf{r}') &\equiv [\hat{C}(\mathbf{r}, \mathbf{r}')]_{ij} = \langle \psi_i(\mathbf{r}) \psi_j(\mathbf{r}') \rangle \\ &= \int \psi_i(\mathbf{r}) \psi_j(\mathbf{r}') P[\boldsymbol{\psi}] \mathcal{D}\boldsymbol{\psi}. \end{aligned} \quad (15)$$

The correlator (15) is more appropriately known as the 2-point static correlation function [26] and so long as we are within the Gaussian approximation no other correlation functions are required.

For functional integrals, explicit analytical treatment can be rather involved [27, 28]. For our purposes, it is, however, more convenient to modify the distribution (13) by adding a source term to the free energy so as to introduce the generating functional of the correlation functions through the partition function of the modified distribution [26]. The free

energy is now as follows

$$\begin{aligned} F^{(2)}[\boldsymbol{\psi}|\mathbf{J}] &= F_b^{(2)}[\boldsymbol{\psi}|\mathbf{J}] + F_s^{(2)}[\boldsymbol{\psi}] \\ &= F^{(2)}[\boldsymbol{\psi}] - \beta^{-1} \int_V J_i(\mathbf{r}) \psi_i(\mathbf{r}) dv, \end{aligned} \quad (16)$$

where $\mathbf{J} \equiv \begin{pmatrix} J_1 \\ J_2 \end{pmatrix}$. The relation linking the correlator and functional derivatives of the generating functional is

$$\begin{aligned} C_{ij}(\mathbf{r}, \mathbf{r}') &= C_{ij}(\mathbf{r}, \mathbf{r}'|\mathbf{J}) \Big|_{\mathbf{J}=0} \\ &= \frac{\delta^2 \ln Z[\mathbf{J}]}{\delta J_i(\mathbf{r}) \delta J_j(\mathbf{r}')} \Big|_{\mathbf{J}=0} = \frac{\delta \bar{\psi}_i(\mathbf{r}|\mathbf{J})}{\delta J_j(\mathbf{r}')} \Big|_{\mathbf{J}=0}, \end{aligned} \quad (17)$$

where

$$\bar{\psi}_i(\mathbf{r}|\mathbf{J}) = \int \psi_i(\mathbf{r}) P[\boldsymbol{\psi}|\mathbf{J}] \mathcal{D}\boldsymbol{\psi}. \quad (18)$$

In our case all the functional integrals are Gaussian and the saddle point approximation

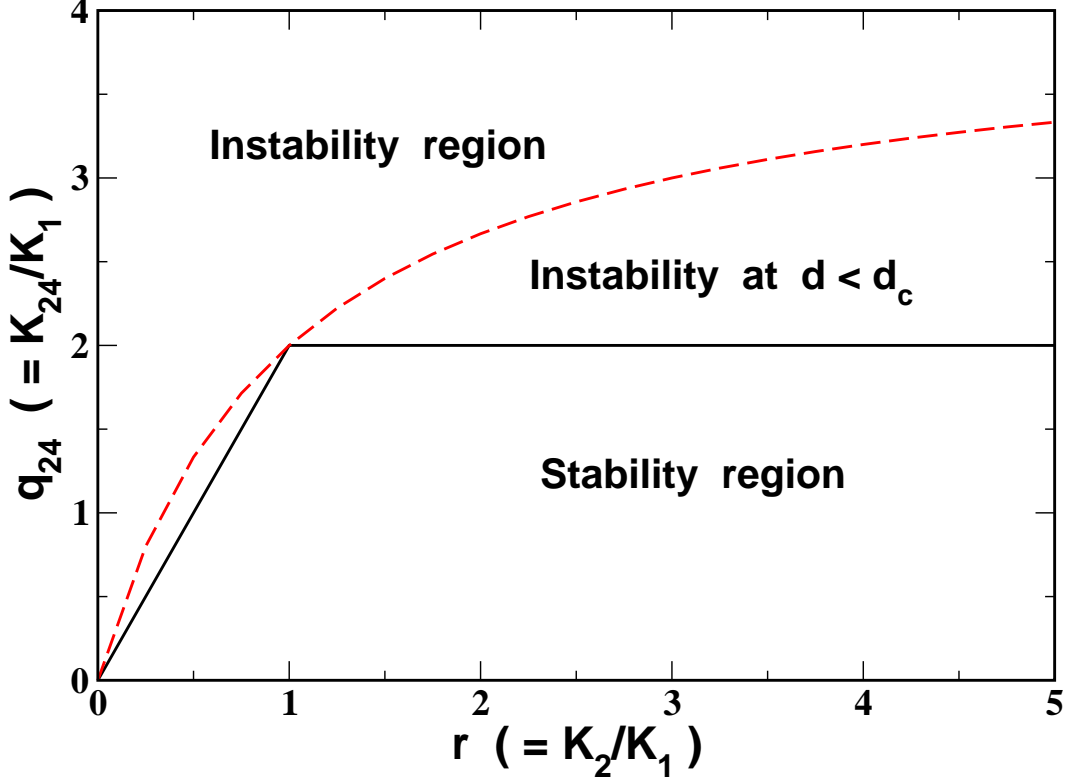


FIG. 3: Stability diagram in the r - q_{24} plane. There are two critical values of q_{24} : $q_c^{(1)}$ (solid line) and $q_c^{(2)}$ (dashed line).

yields the exact results. So, the averaged fluctuation field (18) can be computed as an extremal of the free energy (16) which satisfies the Euler-Lagrange equations

$$\hat{K}_{ij}\bar{\psi}_j(\mathbf{r}|\mathbf{J}) = \beta^{-1}J_i(\mathbf{r}) \quad (19)$$

and meets the boundary conditions

$$\hat{Q}_{ij}\bar{\psi}_j(\mathbf{r}|\mathbf{J})|_{\mathbf{r}\in S} = 0, \quad \hat{Q} = \hat{Q}^{(b)} + \hat{Q}^{(s)}. \quad (20)$$

So long as the boundary value problem (19)–(20) is linear, the fluctuation field (18) linearly depend on the source. This relation is given by

$$\bar{\psi}_i(\mathbf{r}|\mathbf{J}) = \beta^{-1} \int_V G_{ij}(\mathbf{r}, \mathbf{r}') J_j(\mathbf{r}') dv', \quad (21)$$

where \hat{G} is the Green function of the operator \hat{K} . Eqs. (17) and (21) show that the correlator is proportional to the Green function

$$\hat{C}(\mathbf{r}, \mathbf{r}') = \beta^{-1}\hat{G}(\mathbf{r}, \mathbf{r}'). \quad (22)$$

So, in order compute the correlator \hat{C} we need to solve the boundary value problem for the Green function \hat{G} :

$$\hat{K}_{ik}G_{kj}(\mathbf{r}, \mathbf{r}') = \delta(\mathbf{r} - \mathbf{r}')\delta_{ij}, \quad (23a)$$

$$\hat{Q}_{ik}G_{kj}(\mathbf{r}, \mathbf{r}')|_{\mathbf{r}\in S} = 0, \quad (23b)$$

where $\delta(\mathbf{r})$ is the delta function. The problem (23) is at the heart of the conventional computational procedures traditionally used, e.g., in studies of light scattering in confined liquid crystals [29, 30, 31, 32, 33].

The key point is that the effects caused by the anchoring energy and the surface elasticity constant are solely incorporated into the boundary conditions (23b). These conditions affect eigenfunctions (normal fluctuation modes) and eigenvalues of the operator \hat{K} that can be used to derive the Green function in the form of an expansion over the eigenfunctions.

The eigenvalues form the spectrum of fluctuation

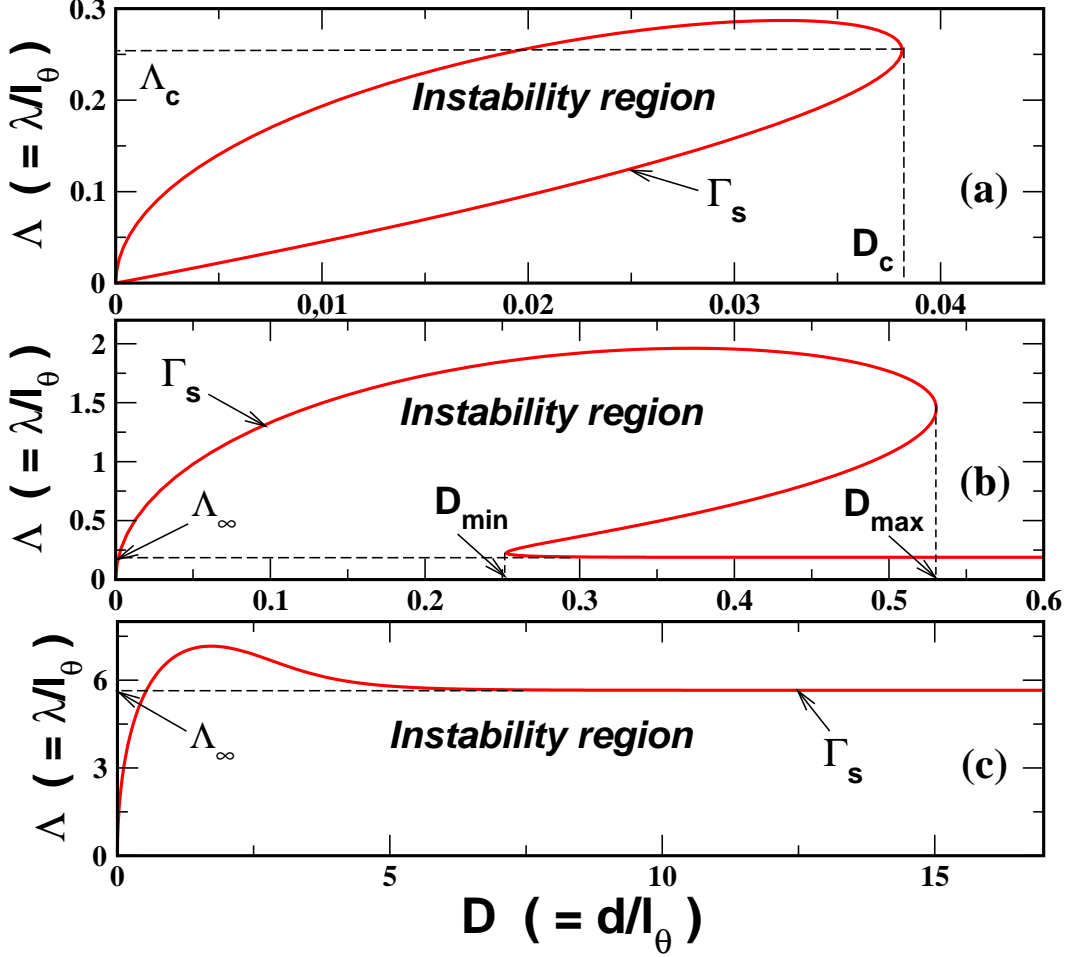


FIG. 4: Stability diagrams in the D - Λ plane at $W_\phi = W_\theta$ and $r \equiv K_2/K_1 = 1.5$ for various values of $q_{24} = K_{24}/K_1$: (a) $q_c^{(1)} = 2 < q_{24} = 2.1 < q_c^{(2)} = 2.4$; (b) $q_c^{(2)} = 2.4 < q_{24} = 2.43 < 2r = 3$; and (c) $2r = 3 < q_{24} = 3.3$.

tuations and must be positive provided the orientational structure \mathbf{n}_0 is stable. Otherwise, the functional integrals (14) and (15) do not converge.

We have thus formulated the spectral stability conditions that turn out to be closely related to the approach based on the generating functional. These conditions are in considerable use as stability criteria in several methods developed to study Fréedericksz-type transitions in confined liquid crystals [34, 35].

C. Surface part of correlator and stability

We now pass on to the approach that emphasize the role of the director fluctuations at the confining surface by using another transformation of the functional integral (15). This transformation has long been known as an efficient method to perform Gaussian integrals [26] and we, following the general idea, define the new integration variable φ_b that vanishes at the surface by translating the fluctuation field ψ :

$$\psi = \varphi_b + \varphi, \quad \varphi_b|_S = 0, \quad (24)$$

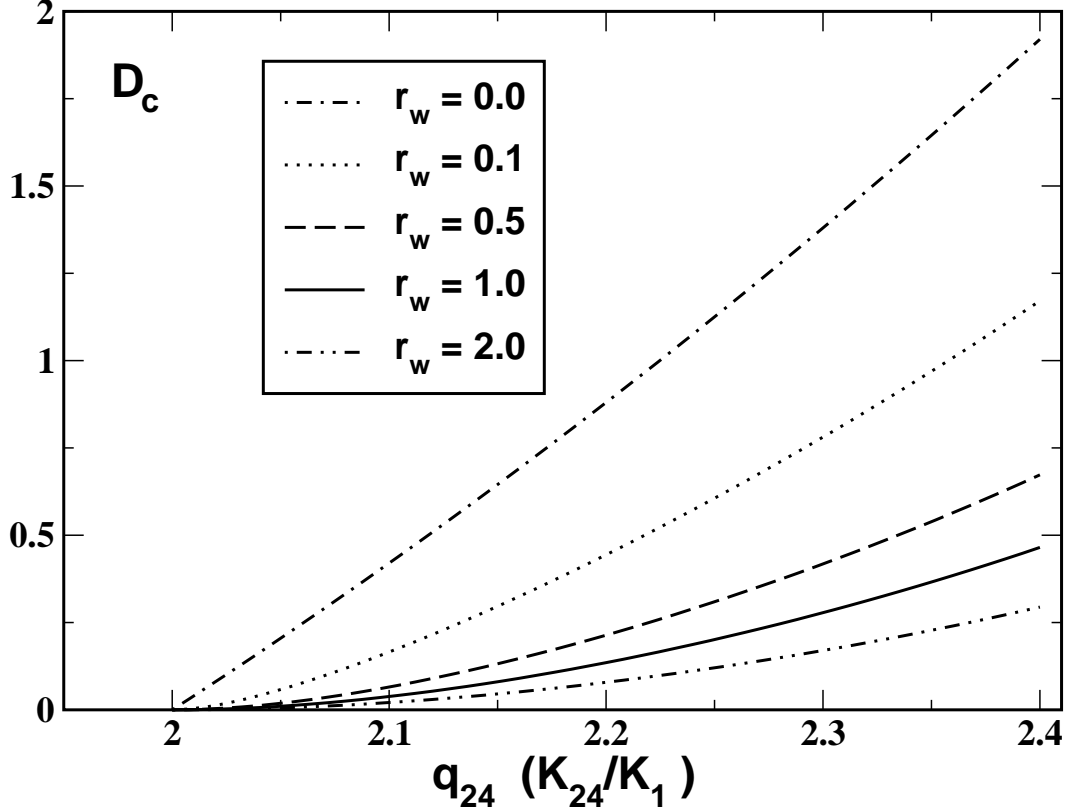


FIG. 5: Dimensionless parameter of critical thickness $D_c (= d_c/l_\theta)$ versus q_{24} at $r = 1.5$ for various values of the azimuthal anchoring parameter $r_w = W_\phi/W_\theta$.

where $\varphi_b = \begin{pmatrix} \varphi_1^{(b)} \\ \varphi_2^{(b)} \end{pmatrix}$.

The fluctuation field ψ is thus decomposed into the field, φ_b , vanishing at the surface and the field φ that accounts for non-vanishing fluctuations at the surface, $\psi|_S = \varphi_s$. When φ additionally satisfies the Euler-Lagrange equations (9)

$$\hat{K}\varphi = 0, \quad \varphi|_S = \psi|_S \equiv \varphi_s, \quad (25)$$

the fluctuations described by φ_b and φ will be statistically independent

$$F^{(2)}[\varphi_b + \varphi] = F_b^{(2)}[\varphi_b] + \Phi_s[\varphi_s], \quad (26)$$

$$\Phi[\varphi_s] = \int_S (\varphi_s, \hat{Q}\varphi_s) ds. \quad (27)$$

Derivation of Eq. (26) relies on the formal properties listed at the end of Sec. II A. It involves using the Green formula (12) and the relation $\hat{Q}^{(s)}\varphi_b|_S = 0$.

From Eqs. (26) and (13) we obtain the probability distributions:

$$P_b[\varphi_b] = Z_b^{-1} \exp\{-\beta F_b^{(2)}[\varphi_b]\}, \quad (28)$$

$$P_s[\varphi_s] = Z_s^{-1} \exp\{-\beta \Phi_s[\varphi_s]\}, \quad (29)$$

where $P_b[\varphi_b]$ is the distribution for the field of fluctuations in the bulk φ_b ; and the distribution $P_s[\varphi_s]$ characterizes the fluctuations at the surface φ_s .

Averaging over the fluctuation fields φ_s and φ_b can now be performed independently. As a result, we have

$$\begin{aligned} \langle A_b A_s \rangle &= \int A_b A_s P[\psi] \mathcal{D}\psi = \int A_s P_s[\varphi_s] \mathcal{D}\varphi_s \\ &\times \int_{\varphi_b|_S=0} A_b P_b[\varphi_b] \mathcal{D}\varphi_b = \langle A_s \rangle_s \langle A_b \rangle_b, \end{aligned} \quad (30)$$

where $A_s \equiv A_s[\varphi_s]$ and $A_b \equiv A_b[\varphi_b]$.

After substituting the decomposition (24) into Eq. (15) and using Eq. (30) to carry out

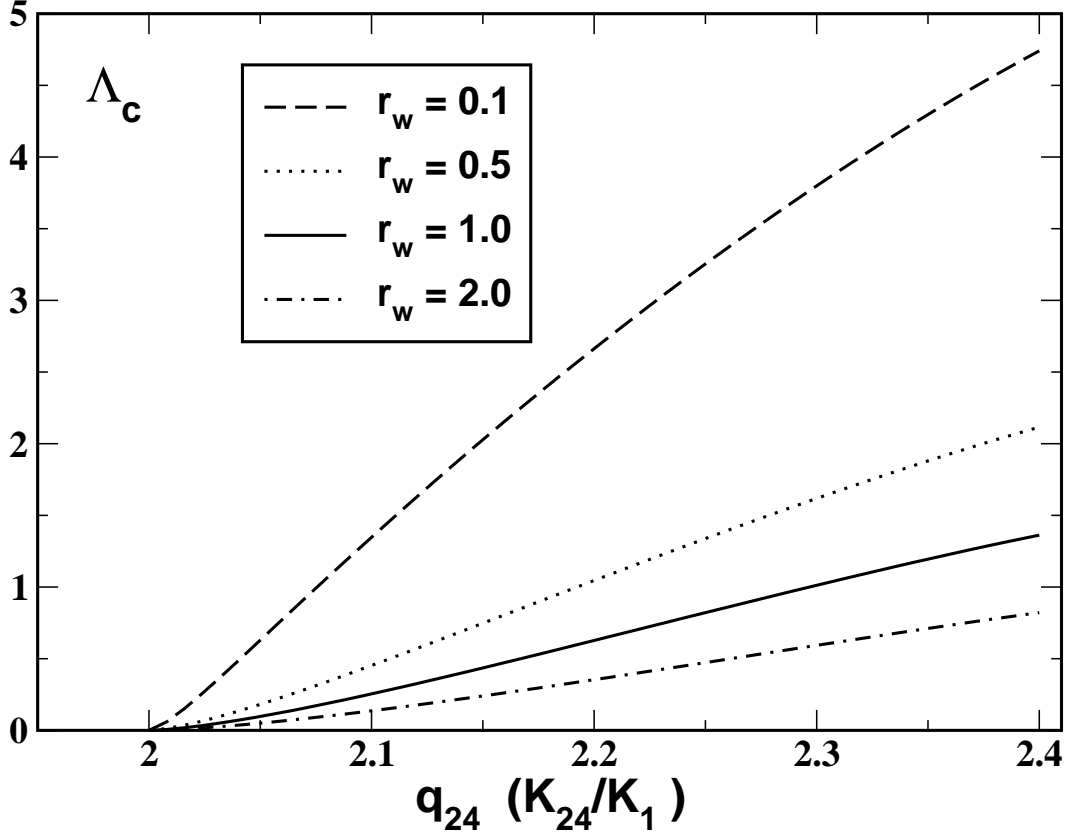


FIG. 6: Dimensionless parameter of critical wavelength $\Lambda_c (= \lambda_c/l_\theta)$ versus q_{24} at $r = K_2/K_1 = 1.5$ for various values of the azimuthal anchoring parameter r_w .

averaging over fluctuations we arrive at the expression for the correlator in the final form

$$C_{ij}(\mathbf{r}, \mathbf{r}') = C_{ij}^{(b)}(\mathbf{r}, \mathbf{r}') + C_{ij}^{(s)}(\mathbf{r}, \mathbf{r}'). \quad (31)$$

The two terms on the right hand side of Eq. (31) are given by

$$C_{ij}^{(b)}(\mathbf{r}, \mathbf{r}') = \langle \varphi_i^{(b)}(\mathbf{r}) \varphi_j^{(b)}(\mathbf{r}') \rangle_b, \quad (32)$$

$$C_{ij}^{(s)}(\mathbf{r}, \mathbf{r}') = \langle \varphi_i(\mathbf{r} | \varphi_s) \varphi_j(\mathbf{r}' | \varphi_s) \rangle_s, \quad (33)$$

where notations for the argument of φ indicate the dependence of the field φ on φ_s (see Eq. (25)).

The correlator $\hat{C}^{(b)}$ is entirely determined by the bulk director fluctuations with the probability distribution (28). In this case the fluctuations at the surface are suppressed and the boundary conditions for $\hat{C}^{(b)}$ are

$$C_{ij}^{(b)}(\mathbf{r}, \mathbf{r}')|_{\mathbf{r} \in S} = 0. \quad (34)$$

These conditions can be described as the limit of infinitely strong anchoring for Eq. (23b). The result is that $\hat{C} = \hat{C}^{(b)}$ in the case of strong anchoring.

When the anchoring is not infinitely strong, the boundary conditions (23b) differ from the strong anchoring conditions (34). Now the fluctuations at the confining wall have not been suppressed completely and are characterized by the probability distribution (29) with the free energy (27). Eq. (25) shows that these fluctuations transmitted into the bulk give rise to the fluctuation field φ . Eq. (33) gives the correlator of the field φ induced by the fluctuations at the surface and determines the difference between \hat{C} and $\hat{C}^{(b)}$. In what follows the correlator $\hat{C}^{(s)}$ will be referred to as the surface part of the correlator \hat{C} .

It is of particular interest that the surface

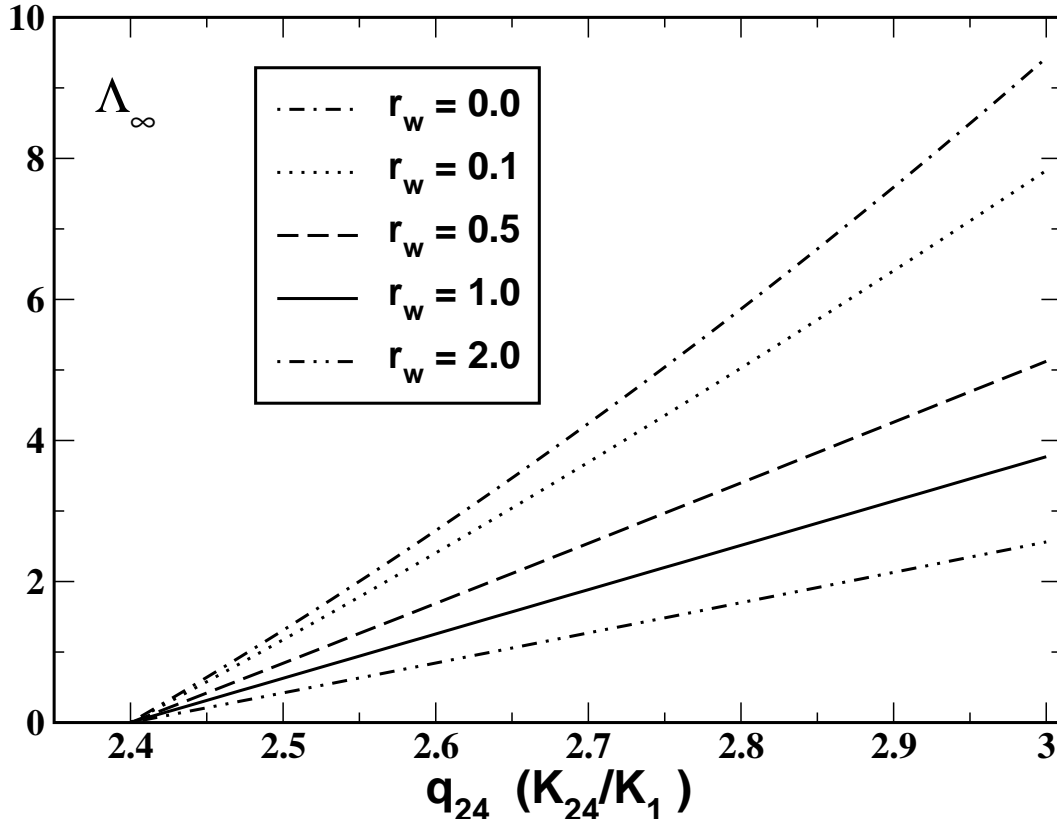


FIG. 7: Dimensionless parameter of critical asymptotic wavelength Λ_∞ ($= \lambda_\infty/l_\theta$) versus q_{24} at $r = K_2/K_1 = 1.5$ for various values of the azimuthal anchoring parameter r_w .

part of the correlator is written as an average with the distribution (29). When the free energy (27) is not positive definite and the conditions

$$(\varphi_s, \hat{Q}\varphi_s) > 0 \quad (35)$$

are violated, the correlator (33) becomes divergent. So, stability of the orientational structure with respect to the director fluctuations at the confining surface is determined by the stability conditions (35). Instabilities induced by such fluctuations are of our primary concern, since neither the anchoring energy nor the K_{24} term may affect the correlator of the bulk fluctuation field (32).

Technically, using the conditions (35) enormously simplifies stability analysis as compared to exploring the spectrum of fluctuations [35]. The procedure involves two steps: (a) solving the boundary value problem for the Euler-Lagrange equations (25);

and (b) evaluating the free energy of the fluctuations at the surface (27). Finally, the stability conditions are derived as the conditions for the free energy to be positive definite.

Equivalent computational schemes have already been used to study surface elasticity effects in Refs. [21, 25, 36]. We have thus developed the method at the very least linking these schemes and the surface part of the correlator that takes into account the director fluctuations at the confining surface.

In the next section we apply the above described procedure to the case of the planar orientational structure in NLC cell. As an advantage of our approach, the study of the fluctuations at the bounding plates will be naturally incorporated into the stability analysis

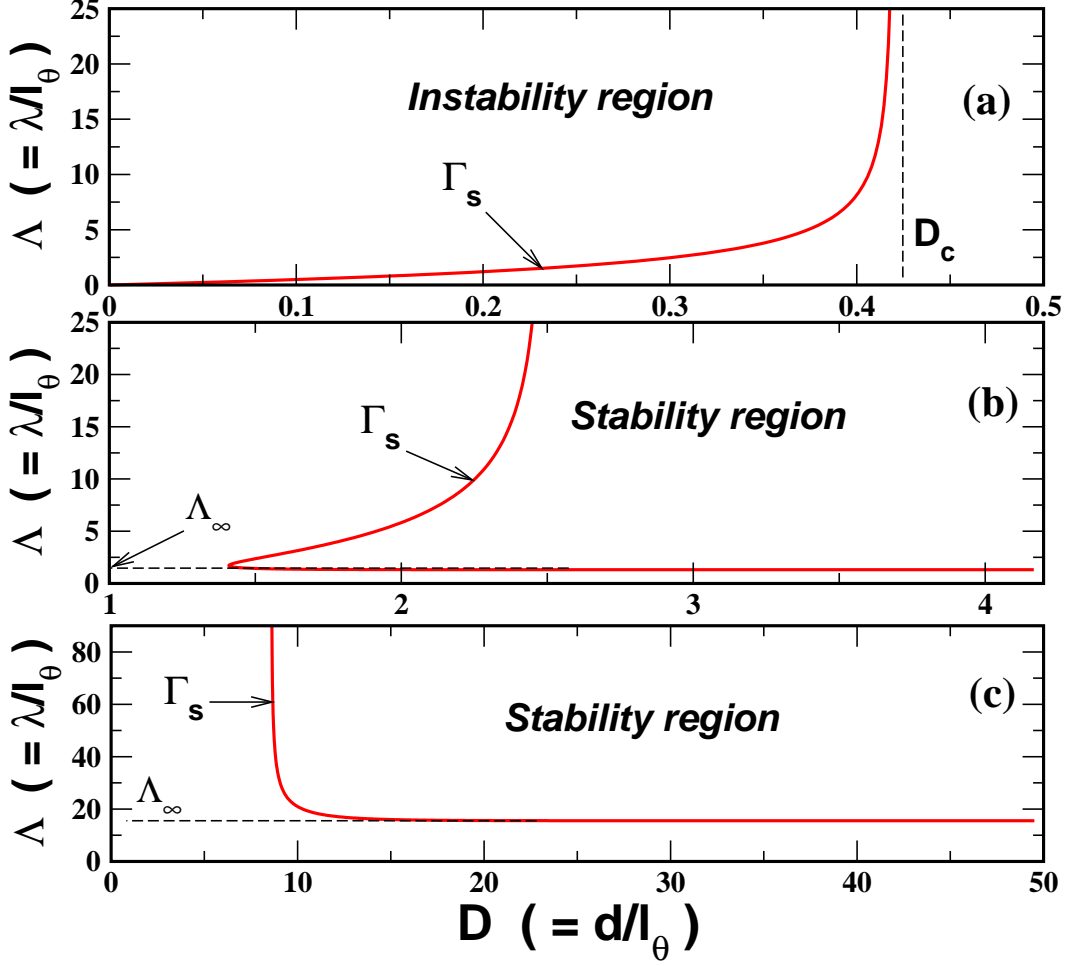


FIG. 8: Stability diagrams in the D - Λ plane at $W_\phi = 0$ and $r = 1.5$ for various values of q_{24} : (a) $q_c^{(1)} = 2 < q_{24} = 2.1 < q_c^{(2)} = 2.4$; (b) $q_c^{(2)} = 2.4 < q_{24} = 2.5 < 2r = 3$; and (c) $2r = 3 < q_{24} = 3.3$.

III. DIRECTOR FLUCTUATIONS IN NEMATIC CELL

In this section we consider a NLC planar cell of the thickness d sandwiched between two substrates that are both normal to the z axis: $z = -d/2$ and $z = d/2$. Anchoring conditions at both substrates are planar with the vector of the easy orientation directed along the x axis. Thus, the uniform planar director distribution $\mathbf{n}_0 = \mathbf{e}_x$ gives the undistorted orientational structure.

The distorted director (5) with $\mathbf{n}_1 = \mathbf{e}_y$ and $\mathbf{n}_2 = \mathbf{e}_z$ is characterized by the angles ϕ and θ shown in Fig. 1. For small angles, the approximate second order expression for the

anchoring potential is

$$W(\mathbf{n}) \approx W(\mathbf{n}_0) + W_\theta \theta^2 + W_\phi \phi^2, \quad (36)$$

where W_θ and W_ϕ are the zenithal (polar) and the azimuthal anchoring strengths. Note that Eq. (36) does not imply using the Rapini-Papoular potential [37], where $W_\theta = W_\phi$. It is, however, more reasonable to consider the case in which the zenithal and the azimuthal anchoring energies differ, because the surface energy costs for splay-bend and twist director deformations in interfacial layers are different (recent discussion can be found in Ref. [38]).

The cell is invariant under translations in the x - y plane and we impose the pe-

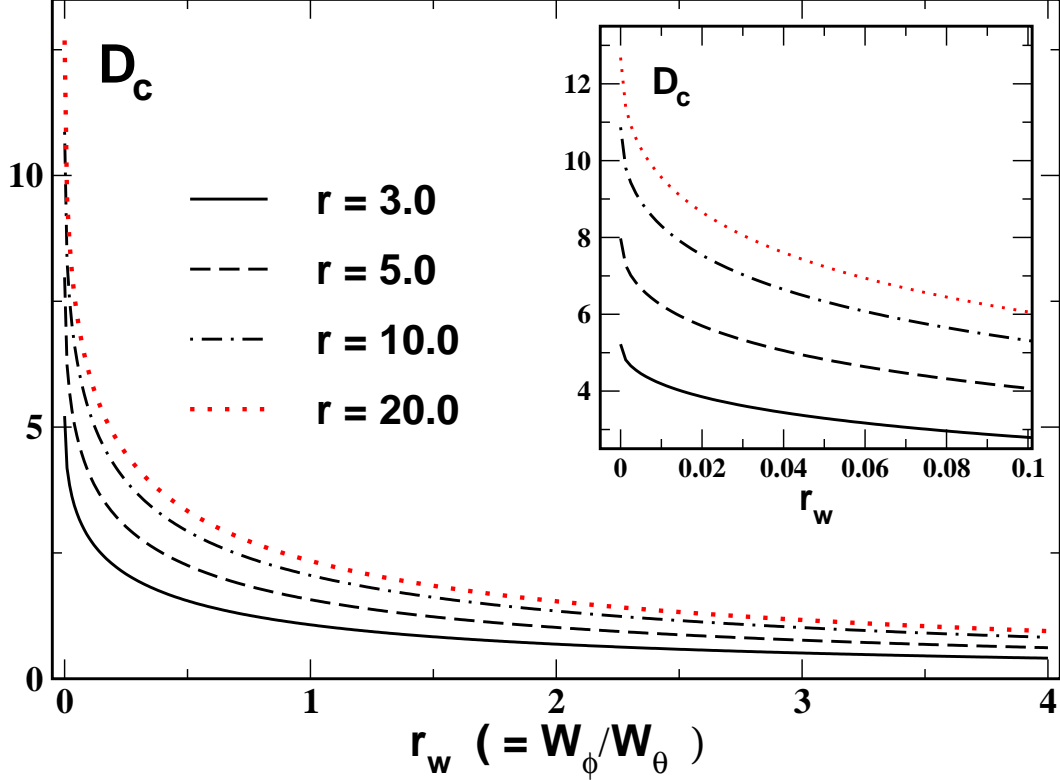


FIG. 9: Dimensionless parameter of critical thickness $D_c (= d_c/l_\theta)$ versus r_w at $q_{24} = q_c^{(2)} - 0.1$ for various values of the elastic anisotropy parameter r . Insert at the upper right corner enlarges initial decay in the neighborhood of the origin.

riodic conditions on the angles: $\psi(x + L_x, y, z) = \psi(x, y, z)$ and $\psi(x, y + L_y, z) = \psi(x, y, z)$, where L_x and L_y are the characteristic lengths of the cell along the x and y axes, respectively. We can now write down the Fourier series expansion for the fluctuations:

$$\psi = \sum_{\mathbf{m}, m_y \geq 0} \{ \psi_{\mathbf{m}}(z) \exp[i(k_x x + k_y y)] + \psi_{\mathbf{m}}^*(z) \exp[-i(k_x x + k_y y)] \}, \quad (37)$$

where $\mathbf{m} = (m_x, m_y)$, $k_x = 2\pi m_x/L_x$, $k_y = 2\pi m_y/L_y$ and an asterisk indicate complex conjugation.

As is shown in Appendix A, the fluctuation harmonics with non-vanishing k_x do not produce additional instability. So, we shall restrict ourselves to the case in which $k_x = 0$. Owing to the translational symmetry, the fluctuation harmonics are statistically independent in the Gaussian approximation and

the free energy of fluctuations takes the form of a sum of the energies of the fluctuation modes:

$$F^{(2)}[\psi] = \sum_{m \geq 0} (2 - \delta_{m,0}) F_m^{(2)}[\psi_m], \quad (38)$$

where $m \equiv m_y$.

Calculation of the free energy is rather straightforward (some details and related comments are given Appendix A) and we present the result in matrix notations for the modified fluctuation harmonics:

$$\psi_m \rightarrow \psi = \begin{pmatrix} 1 & 0 \\ 0 & i \end{pmatrix} \psi_m. \quad (39)$$

For brevity, we drop the index m from notations for the fluctuation field. The energy then can be written in the form

$$F_m^{(2)}[\psi] = \frac{K_1 S}{d} \{ S_m^{(b)}[\psi] + S_m^{(s)}[\psi] \}, \quad (40)$$

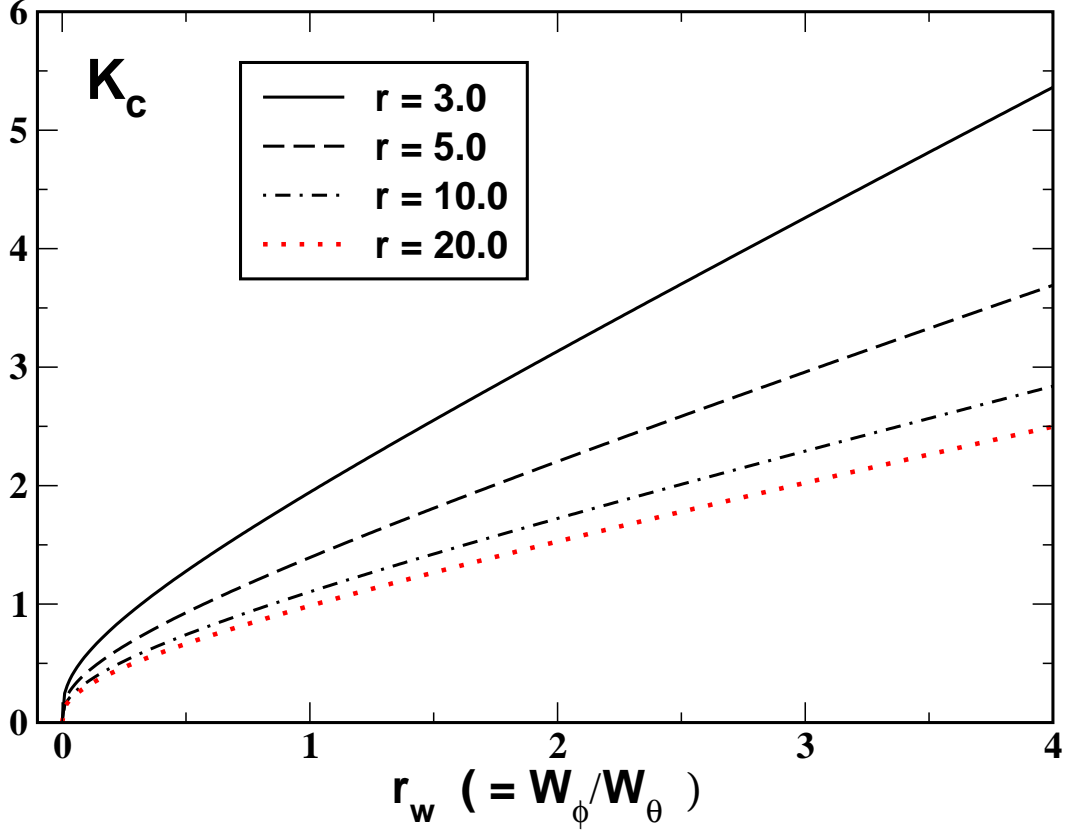


FIG. 10: Dimensionless parameter of critical wavenumber $K_c (= 2\pi/\Lambda_c = k_c l_\theta)$ versus r_w at $q_{24} = q_c^{(2)} - 0.1$ for various values of the elastic anisotropy parameter r .

$$S_m^{(b)}[\psi] = u \int_{-u}^u d\tau \left[[\partial_\tau \psi]^+ \hat{A} \partial_\tau \psi + \frac{1}{2} \psi^+ \hat{B} \partial_\tau \psi + \frac{1}{2} [\partial_\tau \psi]^+ \hat{B}^+ \psi + \psi^+ \hat{C} \psi \right], \quad (41)$$

where $S = L_x L_y$ is the area of the substrates; $\partial_\tau \equiv \frac{\partial}{\partial \tau}$ and a cross indicate Hermitian conjugation. The dimensionless parameters used in Eqs. (41)–(44) are:

$$S_m^{(s)}[\psi] = \sum_{\mu=\pm 1} \psi^+ \hat{Q}_\mu^{(s)} \psi \Big|_{\tau=\mu u}, \quad (42) \quad \tau = k_y z, \quad r = \frac{K_2}{K_1}, \quad q_{24} = \frac{K_{24}}{K_1}, \quad (46)$$

$$u = \frac{k_y d}{2}, \quad w_{\phi, \theta} = \frac{W_{\phi, \theta} d}{2K_1} = \frac{d}{2l_{\phi, \theta}}, \quad (47)$$

$$\hat{A} = \begin{pmatrix} r & 0 \\ 0 & 1 \end{pmatrix}, \quad \hat{C} = \begin{pmatrix} 1 & 0 \\ 0 & r \end{pmatrix}, \quad (43)$$

$$\hat{B} = (r-1) \begin{pmatrix} 0 & 1 \\ -1 & 0 \end{pmatrix}, \quad (44)$$

$$\hat{Q}_\mu^{(s)} = \mu u (q_{24} - (1+r)/2) \begin{pmatrix} 0 & 1 \\ 1 & 0 \end{pmatrix} + \begin{pmatrix} w_\phi & 0 \\ 0 & w_\theta \end{pmatrix}, \quad (45)$$

where l_θ and l_ϕ are the zenithal and the azimuthal anchoring extrapolation lengths, respectively.

A. Mirror symmetry and parity of fluctuations

In order to evaluate the correlator of director fluctuations and study the stability of the planar structure, $\mathbf{n}_0 = \mathbf{e}_x$, we shall need

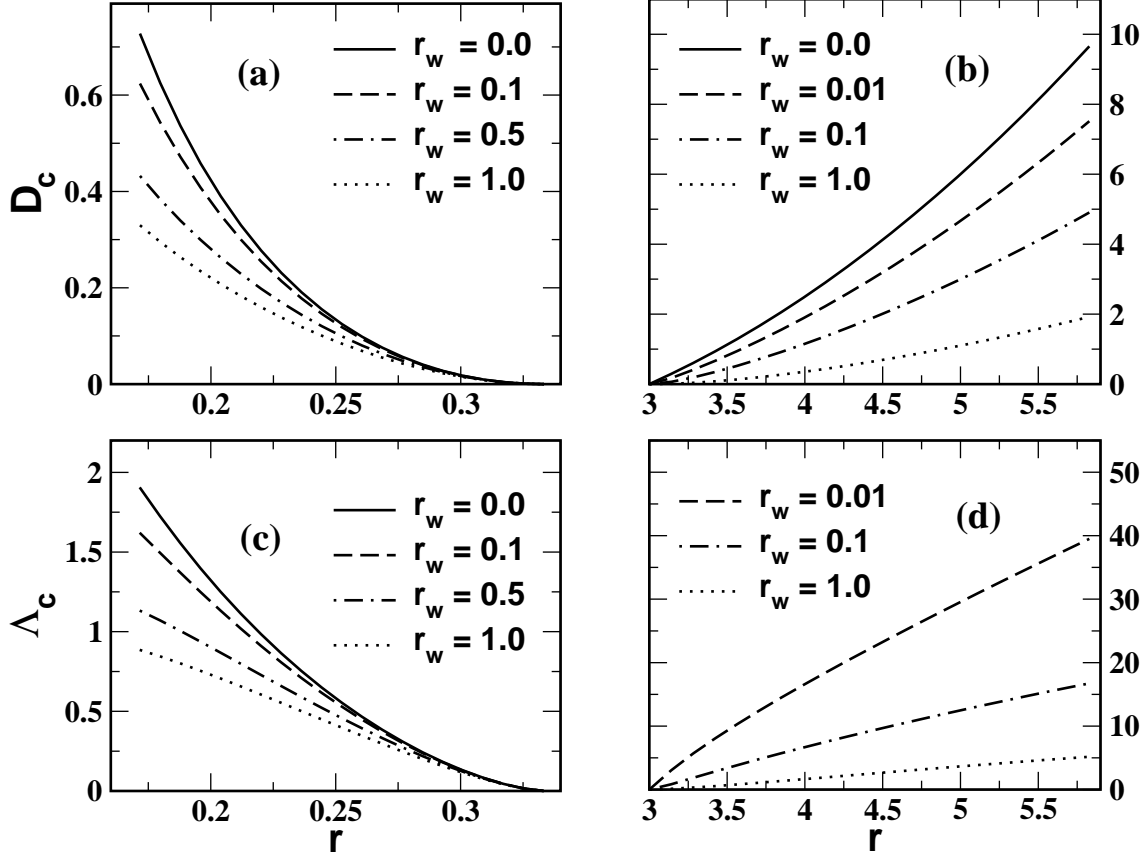


FIG. 11: (a)-(b) The critical thickness and (c)-(d) the critical wavelength parameters as a function of the twist-splay ratio r for various values of r_w . The graphs are computed by using the Cauchy relation: $q_{24} = (1+r)/2$. The saddle-splay parameter q_{24} is in the instability region (88) when r lies in the intervals: $3 - 2\sqrt{2} < r < 1/3$ or $3 < r < 3 + 2\sqrt{2}$.

to solve the Euler-Lagrange equations for the fluctuation free energy functional (40):

$$\hat{L}\varphi = 0, \quad (48)$$

$$\hat{L} = \hat{A}\partial_\tau^2 - \hat{B}\partial_\tau - \hat{C}. \quad (49)$$

These equations are invariant under the mirror symmetry transformation [21]:

$$\varphi(\tau) \rightarrow \hat{P}\varphi(-\tau), \quad \hat{P} = \begin{pmatrix} 1 & 0 \\ 0 & -1 \end{pmatrix} \quad (50)$$

Algebraically, this result follows because the matrices \hat{P} , \hat{A} and \hat{C} are commuting, $\hat{P}\hat{A} - \hat{A}\hat{P} = \hat{P}\hat{C} - \hat{C}\hat{P} = 0$, whereas the matrices \hat{P} and \hat{B} anticommute, $\hat{P}\hat{B} + \hat{B}\hat{P} = 0$.

The identity $\hat{P}^2 = \hat{I}$, where \hat{I} is the identity matrix, shows that invariant sets of the

solutions of Eq. (48) can be characterized by the parity with respect to the transformation (50):

$$\psi_{s,a}(-\tau) = \pm \hat{P}\psi_{s,a}(\tau), \quad (51)$$

where ψ_s and ψ_a will be referred to as the symmetric and the antisymmetric fluctuation modes, respectively. For symmetric [antisymmetric] fluctuation fields, the parity relation (51) means that the in-plane and the out-of-plane components, ϕ and θ , are represented by even [odd] and odd [even] functions of τ , correspondingly: $\phi(-\tau) = \phi(\tau)$ [$\phi(-\tau) = -\phi(\tau)$] and $\theta(-\tau) = -\theta(\tau)$ [$\theta(-\tau) = \theta(\tau)$].

The general solution is now a sum of the

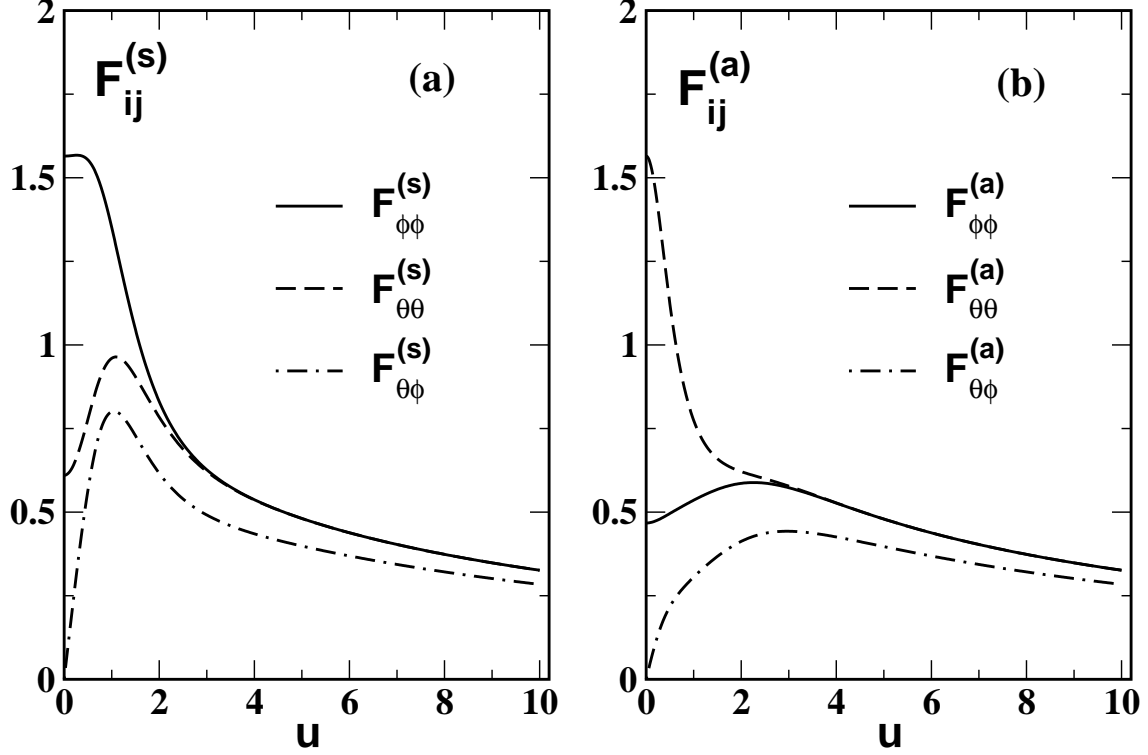


FIG. 12: Elements of the covariance matrix (75) as functions of u ($= k_y d/2$) for (a) symmetric and (b) antisymmetric fluctuations at the lower substrate, $z = -d/2$. The thickness parameter $D = D_c + 1.0 = 1.27$ is noticeably above its critical value $D_c = 0.27$ at $q_{24} = q_c^{(1)} + 0.3 = 1.7 < q_c^{(2)}$, $r = 1.5$ and $r_w = 1.0$.

symmetric and the antisymmetric modes:

$$\varphi(\tau) = \psi_s(\tau) + \psi_a(\tau). \quad (52)$$

We shall write expressions for the modes in matrix notations through the two fundamental matrices $\hat{\Psi}^{(s)}(\tau)$ and $\hat{\Psi}^{(a)}(\tau)$ composed from solutions of the corresponding symmetry. These 2×2 matrices satisfy both the Euler-Lagrange equation (48) and the par-

ity relation (51). In addition, $\hat{\Psi}^{(\alpha)}(\tau)$ will be conveniently normalized by the condition: $\hat{\Psi}^{(\alpha)}(u) = \hat{I}$. It can be verified that solving Eq. (48) yields the following result:

$$\psi_\alpha(\tau) = \hat{\Psi}^{(\alpha)}(\tau)\varphi_\alpha, \quad \alpha = s, a, \quad (53)$$

$$\hat{\Psi}^{(\alpha)}(\tau) = \hat{\Phi}_\alpha(\tau)[\hat{\Phi}_\alpha(u)]^{-1}, \quad (54)$$

$$\hat{\Phi}_s(\tau) = \begin{pmatrix} \cosh \tau + \rho\tau \sinh \tau & -\rho\tau \sinh \tau \\ \rho\tau \cosh \tau & \sinh \tau - \rho\tau \cosh \tau \end{pmatrix}, \quad (55a)$$

$$\hat{\Phi}_a(\tau) = \begin{pmatrix} \sinh \tau + \rho\tau \cosh \tau & -\rho\tau \cosh \tau \\ \rho\tau \sinh \tau & \cosh \tau - \rho\tau \sinh \tau \end{pmatrix}, \quad (55b)$$

where φ_α are the vectors of integration constants and

$$\rho = (1 - r)/(1 + r). \quad (56)$$

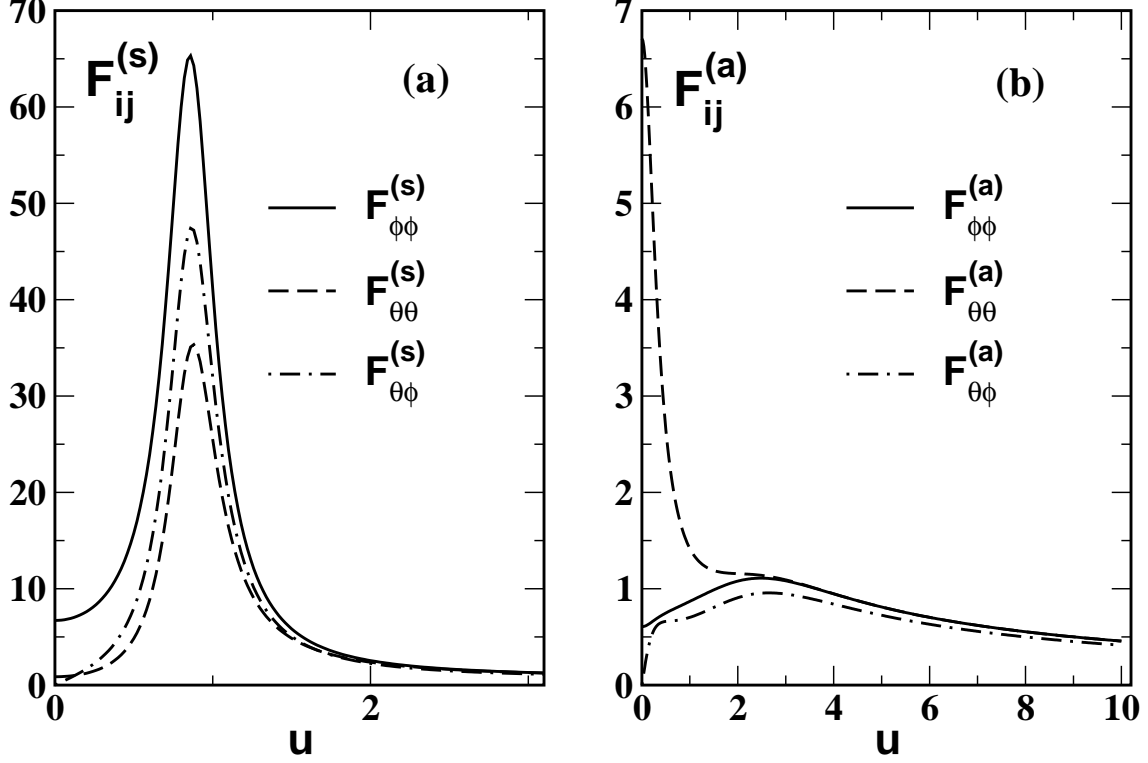


FIG. 13: Elements of the covariance matrix (75) as functions of u ($= k_y d/2$) for (a) symmetric and (b) antisymmetric fluctuations at the lower substrate, $z = -d/2$. The thickness parameter $D = D_c + 0.02 = 0.29$ is in the immediate vicinity of its critical value $D_c = 0.27$ at $q_{24} = q_c^{(1)} + 0.3 = 1.7 < q_c^{(2)}$, $r = 1.5$ and $r_w = 1.0$.

After substituting Eqs. (52)–(53) into Eq. (40) and using the symmetry relation (51), we find that the symmetric and the antisymmetric fluctuations independently contribute to the free energy of the fluctuation field (52):

$$F_m^{(2)}[\varphi] = \frac{2K_1 S}{d} (\varphi_s^+ \hat{M}_s \varphi_s + \varphi_a^+ \hat{M}_a \varphi_a), \quad (57)$$

$$\hat{M}_\alpha = u \left(\hat{A} \partial_\tau \hat{\Psi}^{(\alpha)} \Big|_{\tau=u} - \frac{1}{2} \hat{B} \right) + \hat{Q}_+^{(s)}. \quad (58)$$

We can now combine Eqs. (43)–(45) and Eqs. (54)–(56) to derive expressions for the matrices \hat{M}_s and \hat{M}_a from Eq. (58). The result is given by

$$\hat{M}_s = \frac{1}{\beta_s} \begin{pmatrix} (1-\rho)u \tanh^2 u + w_\phi \beta_s & u(q_{24} \beta_s - (1-\rho) \tanh u) \\ u(q_{24} \beta_s - (1-\rho) \tanh u) & (1-\rho)u + w_\theta \beta_s \end{pmatrix}, \quad (59a)$$

$$\hat{M}_a = \frac{1}{\beta_a} \begin{pmatrix} (1-\rho)u + w_\phi \beta_a & u(q_{24} \beta_a - (1-\rho) \tanh u) \\ u(q_{24} \beta_a - (1-\rho) \tanh u) & (1-\rho)u \tanh^2 u + w_\theta \beta_a \end{pmatrix}, \quad (59b)$$

where

$$\beta_{s,a} = \tanh u \mp \rho u (1 - \tanh^2 u). \quad (60)$$

B. Director fluctuations at substrates

Now we apply the analytical results of Sec. IIIB to evaluate the energy of fluctuation harmonics at the substrates and the surface part of the correlation function. According to the procedure described in Sec. IIC, the first step is to solve the boundary value problem (25).

To this end we shall find the fluctuation field that satisfies the Euler-Lagrange equations (48) and the boundary conditions

$$\varphi(\pm u) = \varphi^{(\pm)}, \quad (61)$$

where $\varphi^{(+)}$ [$\varphi^{(-)}$] is the value of the fluctuation field at the upper [lower] substrate of the cell. By analogy with the representation given in Eqs. (52) and (53), we can write the field in the form

$$\varphi(\tau) = \hat{\Psi}^{(+)}(\tau)\varphi^{(+)} + \hat{\Psi}^{(-)}(\tau)\varphi^{(-)}, \quad (62)$$

$$\hat{\Psi}^{(\mu)}(\nu u) = \delta_{\mu\nu}\hat{I}, \quad \mu, \nu = \pm 1, \quad (63)$$

where the matrices $\hat{\Psi}^{(+)}$ and $\hat{\Psi}^{(-)}$ are the solutions of the Euler-Lagrange equation (48) that are equal to the identity matrix at one substrate and vanish at the other.

It can be readily verified that $\hat{\Psi}^{(+)}$ and $\hat{\Psi}^{(-)}$ are related to the matrices derived in Eqs. (54)–(55b) through the linear combinations

$$\hat{\Psi}^{(+)} = \frac{1}{2} \{ \hat{\Psi}^{(s)} + \hat{\Psi}^{(a)} \}, \quad (64a)$$

$$\hat{\Psi}^{(-)} = \frac{1}{2} \{ \hat{\Psi}^{(s)} - \hat{\Psi}^{(a)} \} \hat{P}. \quad (64b)$$

The fluctuation field (62) thus has been defined.

Clearly, Eq. (62) and Eq. (52) present the fluctuation field φ in two different forms. This in combination with Eqs. (64a)–(64b)

yields the relation between the vectors $\varphi^{(\pm)}$ and $\varphi_{s,a}$:

$$\phi \equiv \begin{pmatrix} \varphi^{(+)} \\ \varphi^{(-)} \end{pmatrix} = \hat{T} \begin{pmatrix} \varphi_s \\ \varphi_a \end{pmatrix}, \quad (65)$$

where $\hat{T} = \begin{pmatrix} \hat{I} & \hat{I} \\ \hat{P} & -\hat{P} \end{pmatrix}$.

The general expression for the energy of fluctuations at the surfaces has been derived in Eq. (27). In our case this energy is a quadratic form of the boundary values of the fluctuation field (62), $\varphi^{(+)}$ and $\varphi^{(-)}$, that can be evaluated by substituting Eq. (62) into Eq. (40). From the other hand, the energy expressed in terms of φ_s and φ_a has already been obtained in Eq. (57). So, with the relation (65) we are left with the following result

$$\begin{aligned} \Phi_m^{(s)}(\varphi^{(+)}, \varphi^{(-)}) &= F_m^{(2)}[\varphi] \\ &= \frac{K_1 S}{d} \phi^+ \hat{N} \phi, \end{aligned} \quad (66)$$

$$\hat{T}^+ \hat{N} \hat{T} = 2 \begin{pmatrix} \hat{M}_s & 0 \\ 0 & \hat{M}_a \end{pmatrix}, \quad (67)$$

where the matrix \hat{N} is described in Appendix B (see Eqs. (B3)–(B5)).

After substituting the fluctuation field into the expression for the surface part of the correlator (33) we have

$$\begin{aligned} C_{ij}^{(s)}(\tau, \tau') &= \langle \varphi_i(\tau) \varphi_j(\tau') \rangle_s \\ &= \Psi_{im}^{(\mu)}(\tau) D_{mn}^{(\mu\nu)} \Psi_{nj}^{(\nu)}(\tau') \end{aligned} \quad (68)$$

where $D_{mn}^{(\mu\nu)} \equiv \langle \varphi_m^{(\mu)} \varphi_n^{(\nu)} \rangle_s$. In our case, we can easily carry out the averaging over fluctuations by calculating Gaussian integrals with the probability distribution defined in Eqs. (29) and (66). The result is

$$\hat{D} \equiv \begin{pmatrix} \hat{D}^{(++)} & \hat{D}^{(+-)} \\ \hat{D}^{(-+)} & \hat{D}^{(--)} \end{pmatrix} = \frac{k_B T d}{K_1 S} \hat{N}^{-1}. \quad (69)$$

In Appendix B the Green function method is found to yield the same result.

By using Eqs. (64) and (67) the surface part of the correlator can now be derived

from Eqs. (68)–(69) in the final form:

$$\hat{C}^{(s)}(\tau, \tau') = \frac{k_B T d}{2K_1 S} \hat{F}(\tau, \tau'), \quad (70)$$

$$\begin{aligned} \hat{F}(\tau, \tau') &= \hat{\Psi}^{(s)}(\tau) \hat{M}_s^{-1} [\hat{\Psi}^{(s)}(\tau')]^\dagger \\ &+ \hat{\Psi}^{(a)}(\tau) \hat{M}_a^{-1} [\hat{\Psi}^{(a)}(\tau')]^\dagger. \end{aligned} \quad (71)$$

As is seen from Eq. (71), the surface part of the correlator is a sum of two terms that represent the contributions coming from the symmetric and the antisymmetric fluctuation harmonics at the substrates. The corresponding terms on the right hand side of Eq. (57) provide expressions for the free energies of these harmonics.

We can further emphasize the role of the matrices \hat{M}_s and \hat{M}_a . For this purpose, we consider the case in which $\tau = \tau' = \pm u$. Since $\hat{C}^{(b)}(\pm u, \pm u) = 0$, the covariance matrix of the director fluctuations at the upper and lower substrates is determined by the correlator (70):

$$\begin{aligned} \hat{C}^{(s)}(\pm u, \pm u) &= \hat{C}(\pm u, \pm u) \\ &= \begin{pmatrix} \langle \phi^2 \rangle & \langle \theta \phi \rangle \\ \langle \theta \phi \rangle & \langle \theta^2 \rangle \end{pmatrix} \Bigg|_{z=\pm d/2}. \end{aligned} \quad (72)$$

From Eq. (71) we have

$$\hat{F}(u, u) = \hat{M}_s^{-1} + \hat{M}_a^{-1}, \quad (73)$$

$$\hat{F}(-u, -u) = \hat{P}(\hat{M}_s^{-1} + \hat{M}_a^{-1})\hat{P}. \quad (74)$$

The fluctuations at the substrates are thus entirely described by the matrices \hat{M}_s and \hat{M}_a . In Sec. IV D we shall discuss symmetric and antisymmetric fluctuations at the lower substrate of the cell and present some numerical results for the elements of the matrix

$$\hat{P} \hat{M}_\alpha^{-1} \hat{P} = \begin{pmatrix} F_{\phi\phi}^{(\alpha)} & F_{\theta\phi}^{(\alpha)} \\ F_{\theta\phi}^{(\alpha)} & F_{\theta\theta}^{(\alpha)} \end{pmatrix}. \quad (75)$$

From Eqs. (70) and (74) this matrix is proportional to the contribution of the corresponding fluctuation mode to the covariance matrix (72).

IV. STABILITY OF PLANAR STRUCTURE

It is now our task to study the stability of the planar structure. In the preceding section we have derived all the analytical results required to perform analysis of the stability conditions (35) efficiently. In our case violating these conditions will render the surface part of the correlator $\hat{C}^{(s)}$ divergent because the free energy (66) is not positive definite and the corresponding Gaussian integrals diverge.

Equivalently, Eqs. (67) and (57) show that the planar structure is stable only if the matrices \hat{M}_s and \hat{M}_a are both positive definite. This yields the following two stability conditions:

$$\det \hat{M}_s > 0 \quad \text{and} \quad \det \hat{M}_a > 0, \quad (76)$$

that determine stability with respect the symmetric and the antisymmetric fluctuation modes.

In order to proceed with our analysis we shall need to write down the expressions for the determinants. From Eqs. (59a) and (59b) we have

$$\begin{aligned} \det \hat{M}_s &= w_\theta w_\phi + \frac{(1-\rho)u}{\beta_s(u)} (w_\theta \tanh^2 u + w_\phi) \\ &- u^2 q_{24} \left(q_{24} - 2 \frac{(1-\rho) \tanh u}{\beta_s(u)} \right), \end{aligned} \quad (77)$$

$$\begin{aligned} \det \hat{M}_a &= w_\theta w_\phi + \frac{(1-\rho)u}{\beta_a(u)} (w_\phi \tanh^2 u + w_\theta) \\ &- u^2 q_{24} \left(q_{24} - 2 \frac{(1-\rho) \tanh u}{\beta_a(u)} \right). \end{aligned} \quad (78)$$

The determinants are written in the form of a sum of three terms, so that only the last term can be negative (the functions $\beta_{s,a}(u)$ are defined in Eq. (60) and cannot be negative).

This term is always negative at $q_{24} < 0$ and we concentrate on the case of our primary concern in which q_{24} is positive. In this case the term will be negative if the inequal-

ity

$$q_{24} > \gamma_\alpha(u) \equiv 2 \frac{(1-\rho) \tanh u}{\beta_\alpha(u)} \quad (79)$$

is fulfilled. Given the value of q_{24} , the values of the parameter u that satisfy the instability condition (79) form the instability interval for the corresponding fluctuation harmonics.

A. General method

The key point underlying our analysis is that the determinant $\det \hat{M}_\alpha$ will be negative provided the cell is sufficiently thin and the parameter u lies within the instability interval. The reasoning is as follows.

Given the parameter u ($= k_y d/2$), that meets the condition (79), the thickness of the cell d , that enters Eqs. (77)–(78) through the parameters $w_\theta = d/(2l_\theta)$ and $w_\phi = d/(2l_\phi)$, can be changed independently by varying the fluctuation wavenumber k_y so as to keep the parameter u fixed. By this means the first two positive terms on the right hand sides of Eqs. (77)–(78) can be reduced to the limit where the sign of the total sum is determined by the last negative term.

From the above discussion it follows that each value of u from the instability interval defines the critical point where the determinant of the critical mode vanishes. This point is characterized by the thickness of the cell and the fluctuation wavelength, $\lambda = 2\pi/k_y$. The thickness can be computed as a function of u by finding the positive root of the quadratic equation $\det \hat{M}_\alpha = 0$. The wavelength then can be found from the relation $u = k_y d/2 = \pi d/\lambda$ (see Eq. (47)).

Geometrically, these calculations give a set of points (d, λ) in the thickness–wavelength plane and by this means the instability interval turned out to be mapped onto the curve Γ_α in the d – λ plane. This curve represents the boundary of the instability region for the corresponding fluctuation harmonics.

It is now rather straightforward to carry out the described procedure and derive the

parametric equations for the curve Γ_α in the form

$$\Gamma_\alpha = \begin{cases} D = x_\alpha(u) = u\lambda_\alpha(u)/\pi, \\ \Lambda = \lambda_\alpha(u), \end{cases} \quad (80)$$

$$\lambda_s(u) = \frac{\pi}{r_w \beta_s(u)} \left\{ -(1-\rho)(\tanh^2 u + r_w) + [(1-\rho)^2(\tanh^2 u + r_w)^2 + 4r_w \beta_s(u) t_s(u)]^{1/2} \right\}, \quad (81)$$

$$\lambda_a(u) = \frac{\pi}{r_w \beta_a(u)} \left\{ -(1-\rho)(r_w \tanh^2 u + 1) + [(1-\rho)^2(r_w \tanh^2 u + 1)^2 + 4r_w \beta_a(u) t_a(u)]^{1/2} \right\}, \quad (82)$$

where

$$t_\alpha(u) = q_{24} \beta_\alpha(u) (q_{24} - \gamma_\alpha(u)), \quad (83)$$

$$D = \frac{d}{l_\theta}, \quad \Lambda = \frac{\lambda}{l_\theta}, \quad r_w = \frac{W_\phi}{W_\theta}, \quad (84)$$

D is the size parameter; Λ is the wavelength parameter; and r_w is the azimuthal anchoring parameter.

In Eqs. (80)–(83) the thickness and the wavelength are both conveniently scaled by the zenithal anchoring extrapolation length, l_θ , and we shall use these formulas to perform numerical analysis later on. But such analysis is not required for our subsequent discussion.

Eqs. (80)–(83) describe the boundary of the instability region provided the instability interval is not empty. So, we turn back to the instability condition (79) to specify the regions of q_{24} in which the instability may occur. To this end we discuss the behavior of the functions $\gamma_s(u)$ and $\gamma_a(u)$ that enter the right hand side of the inequality (79). The results, illustrated in Fig. 2, are not difficult to obtain analytically.

Fig. 2(a) shows that, if the elastic constant K_2 is smaller than K_1 and $r = K_2/K_1 < 1$, the function γ_a increases from

$\gamma_a(0) = 2r$ asymptotically approaching the value $\gamma_a(\infty) = 4r/(r+1)$ at large u , while γ_s is a decreasing function that varies from $\gamma_s(0) = 2$ to $\gamma_s(\infty) = 4r/(r+1)$. As is seen from Fig. 2(b), in the case where $r > 1$ the functions γ_a and γ_s also monotonically approach the common asymptotic value $\gamma_a(\infty) = \gamma_s(\infty) = 4r/(r+1)$. But now we have $\gamma_a(0) = 2r > \gamma_s(0) = 2$.

At the later stage we will see that there are two qualitatively different regimes of instability depending on whether the instability interval is bounded from above or not. So, we have the two characteristic values of q_{24} :

$$q_c^{(1)} = \min(2, 2r), \quad (85)$$

$$q_c^{(2)} = 2(1 - \rho) = \frac{4r}{r+1}. \quad (86)$$

Now we pass on to discuss the stability of the planar structure in the intervals separated by these values.

B. Stability diagrams

In this section we study the stability of the planar structure by analyzing the behavior of the functions which define the boundary curve (80) of the instability region. Qualitatively, the analysis can be performed without resorting to numerical computations and we shall use the numerical results only for illustrative purposes.

Fig. 2 clearly indicates the interval

$$0 < q_{24} < q_c^{(1)} \quad (87)$$

as the region where the inequalities (79) cannot be satisfied and the structure is stable. The stability conditions (87) are equivalent to the long known Ericksen inequalities (4) derived in Ref. [24]. Fig. 3 shows this stability region in the r - q_{24} plane.

Next we consider the interval

$$q_c^{(1)} < q_{24} < q_c^{(2)}, \quad (88)$$

where, as is demonstrated in Fig. 2(a), the instability takes place at $u < u_{\max}$ for the

critical fluctuation mode which symmetry depends on the parameter r . For relatively small elastic constants K_2 with $r < 1$, this mode is antisymmetric (see Fig. 2(a)). Referring to Fig. 2(b), it can be seen that in the opposite case with $r > 1$ the critical mode is symmetric.

Since the instability interval is bounded, the size parameter D on the boundary curve (80) is described by the function $x_\alpha(u)$ and reaches its maximum, D_c , as u varies from 0 to u_{\max} . It follows that in this regime the planar structure is unstable only in sufficiently thin films and d_c ($D_c = d_c/l_\theta$) is the critical thickness. On the curve Γ_α this critical point is also characterized by the critical fluctuation wavelength λ_c ($\Lambda_c = \lambda_c/l_\theta$).

Since $q_{24} = \gamma_\alpha$ at $u = u_{\max}$, Eqs. (77) and (78) show that the q_{24} dependent term vanishes at $u = 0$ and $u = u_{\max}$. When $W_\theta W_\phi \neq 0$, the result is that $x_\alpha(0) = x_\alpha(u_{\max}) = 0$ and the curve Γ_α forms the loop that encloses the region of instability. Fig. 4(a) illustrates this result for $r = 1.5$ when the boundary curve Γ_s is determined by the symmetric critical fluctuation mode.

Now we consider the case of large q_{24} with

$$q_{24} > q_c^{(2)}. \quad (89)$$

In this case the instability interval is no longer bounded from above. From Fig. 2 it is clear that the instability condition (79) does not impose any restrictions on u for the critical mode, whereas the instability interval for the non-critical mode is: $u > u_{\min}$. Thus, the fluctuation modes both lead to the instability at sufficiently large u . Eqs. (81)–(83) provide the limiting value of the functions $\lambda_s(u)$ and $\lambda_a(u)$ at $u \rightarrow \infty$:

$$\Lambda_\infty = \frac{\pi}{r_w} \left\{ -(1 - \rho)(r_w + 1) + [(1 - \rho)^2 \times (r_w + 1)^2 + 4r_w q_{24}(q_{24} - q_c^{(2)})]^{1/2} \right\}, \quad (90)$$

so that the size parameter, $D = u\lambda_\alpha/\pi$, increases indefinitely in this limit. The result is that the planar structure is unstable at

any thickness of the cell and the instability is caused by the short wavelength fluctuations with $\lambda < \lambda_\infty$. This result equally applies to the case of negative q_{24} .

It should be emphasized that using the continuum elastic theory we are limited to the case where the characteristic length of director distortions is large as compared to a microscopic scale of intermolecular distances. This limitation can be taken into consideration by eliminating the fluctuation harmonics with large wavenumbers, $k_{x,y} > k_{uv} = 2\pi/\lambda_{uv}$, from the Fourier series expansion (37), so that the wavenumber k_{uv} gives the large momentum (ultraviolet) cut-off in the theory. In this approach destabilizing effect of the critical short wavelength fluctuations may only be indicated if λ_∞ is larger than λ_{uv} . Our results are scaled by the zenithal anchoring extrapolation length, l_θ . Assuming that the anchoring is sufficiently weak and $l_\theta \gg \lambda_{uv}$, we conclude that in this case the effect of the cut-off on the accuracy of our results is negligible.

Figs. 4(b-c) illustrate transformations of the stability diagram in the D - Λ plane as q_{24} increases beyond $q_c^{(2)}$ at $r > 1$. The curve of the critical mode Γ_s forms the boundary of the instability region similarly to the case of the interval (88). The curve of the non-critical mode Γ_a resides within this region and is not shown in the figures. Both curves rapidly approach the horizontal asymptote $\Lambda = \Lambda_\infty$.

We show in Fig. 4(b) that, when q_{24} is close to $q_c^{(2)}$, the shape of the curve Γ_s still somewhat resembles the loop developed in the interval (88). There are two points marked as D_{\min} and D_{\max} at which the curve bends and at which the function $x_s(u)$ reaches its local minimum and maximum, correspondingly. Further increase of q_{24} reduces the distance between D_{\min} and D_{\max} and the points finally disappear after merging at sufficiently large q_{24} . Fig. 4(c) presents the stability diagram in this regime.

In general, Fig. 3 qualitatively summarizes

the results of this section for the three different intervals of q_{24} described in Eqs. (87)–(89). The interval (89) was previously indicated as the instability region in Ref. [21] and as the region where modulated structures can exist in Ref. [25].

Our results for the interval (88) show that in this case the instability induced by the K_{24} term in cells of subcritical thickness may also lead to the formation of periodically modulated structures. In addition, the critical wavelength λ_c provides an estimate for the period of the emerging structure near the critical point.

C. Effects of azimuthal anchoring

The critical thickness and the critical wavelength are meaningful only when q_{24} is within the interval (88). By using Eqs. (80)–(83) they both can be computed numerically. The numerical procedure involves two steps: (a) solving the equation $x'_\alpha(u_c) = 0$ to find the maximum of x_α for the critical mode; and (b) evaluating $D_c = x_\alpha(u_c)$ and $\Lambda_c = \lambda_\alpha(u_c)$. We also present the results for Λ_∞ computed from Eq. (90).

The critical thickness parameter, D_c , the critical wavelength parameter, Λ_c , and the parameter Λ_∞ as functions of q_{24} for different values of the azimuthal anchoring parameter, $r_w = W_\phi/W_\theta$, are plotted in Figs. 5, 6 and 7. As it can be expected, the curves demonstrate that the structure becomes less stable as the azimuthal anchoring strength decreases. So, in order to estimate the critical thickness from above, it is instructive to discuss the limit of weak azimuthal anchoring, $W_\phi \rightarrow 0$. This limiting case was considered in Refs. [23, 25] and we clarify some of the results by using our approach.

It is, however, should be stressed that in this case the planar structure is marginally stable with respect to the long wavelength symmetric fluctuations with $k_y = 0$ regardless of K_{24} . Mathematically, it follows because the determinant (77) vanishes at $u = 0$

and $w_\phi = 0$. The reason is that all uniform planar structures are energetically equivalent in the absence of azimuthal anchoring.

Nevertheless, we may apply our method to this case by taking the limit $w_\phi \rightarrow 0$ in Eqs. (80)–(90). In this limit the expressions (81), (82) and (90) assume the simplified form

$$\lambda_s(u) = \frac{2\pi t_s(u)}{(1-\rho)\tanh^2 u}, \quad (91)$$

$$\lambda_a(u) = \frac{2\pi t_a(u)}{(1-\rho)}, \quad (92)$$

$$\Lambda_\infty = \lambda_s(\infty) = \frac{2\pi q_{24}}{1-\rho}(q_{24} - q_c^{(2)}). \quad (93)$$

From Eq. (92) it is seen that the behavior of the antisymmetric harmonics at $u = 0$ does not differ from the case in which $w_\phi \neq 0$ and $\lambda_a(0) = x_a(0) = 0$. But, for the symmetric mode, this is not the case. From Eq. (91) we have $\lambda_s \rightarrow \infty$ at $u \rightarrow 0$ and

$$D_c = x_s(0) = 2q_{24}(q_{24} - 2). \quad (94)$$

When $r > 1$ and the critical mode is symmetric, Eq. (94) provides the exact expression for the critical thickness at $W_\phi = 0$. In Refs. [23, 25] the result (94) has been derived as an approximation.

The stability diagrams in the D – Λ plane at $r > 1$ and $W_\phi = 0$ are shown in Fig. 8. In the opposite case of $r < 1$, so long as $q_{24} < 2$ the diagrams are quite similar to those depicted in Fig. 4. Otherwise, at $q_{24} > 2$, the non-critical symmetric mode will change the stability diagram presented in Fig. 4(c). The result, however, is not too different from the diagram shown in Fig. 8(c).

If the azimuthal anchoring strength is not identically zero, Eq. (94) estimates the critical thickness from above. In particular, substituting $q_c^{(2)}$ into Eq. (94) and taking the limit $r \rightarrow \infty$ we arrive at the conclusion that the critical thickness cannot be larger than $16l_\theta$.

Dependencies of the critical thickness, D_c , and the critical wavenumber, $K_c = 2\pi/\Lambda_c$, on

the ratio $r_w = W_\phi/W_\theta$ for various values of r are plotted in Figs. 9 and 10. As is seen from Fig. 9, the critical thickness declines steeply in the immediate vicinity of the origin. Typically, the critical thickness at $r_w = 0$ appears to be halved at $r_w = 0.1$, so that even for $r = 20.0$ we need very small azimuthal anchoring $r_w \approx 0.03$ to have $D_c \approx 8$ ($d_c \approx 8l_\theta$). Referring to Fig. 10, the critical wavenumber, $K_c = 2\pi/\Lambda_c$, also start growing rapidly, but the effect is less pronounced at large values of r . So, we have $K_c \approx 0.2$ ($k_c \approx 0.2/l_\theta$) at $r_w \approx 0.03$ and $r = 20.0$.

When the saddle-splay elastic constant meets a Cauchy relation: $K_{24} = (K_1 + K_2)/2$ [8, 11], we find the two intervals for the twist-splay ratio where the regime of instability defined in Eq. (88) takes place: $3 < r < 3 + 2\sqrt{2} \approx 5.82$ and $3 - 2\sqrt{2} \approx 0.17 < r < 1/3$. The critical thickness and the critical wavelength as a function of the parameter r varying within these intervals are plotted in Fig. 11.

For $r < 1/3$, the critical fluctuation mode is antisymmetric and Fig. 11(c) shows that the critical wavelength remains finite at $r_w = 0$. Referring to Figs. 11(a)-(b), the critical thickness at $r < 1/3$ is an order of magnitude smaller than in the case where $r > 3$ and the critical mode is symmetric.

According to Ref. [23], the latter presents the case in which the ratio r grows anomalously large due to an increase of the twist constant K_2 in the vicinity of the nematic-smectic- A transition. In this case, the estimate of the critical thickness at $W_\phi = 0.0$ and $q_{24} = q_c^{(2)} \approx 3.41$ ($r \approx 5.82$) provides the upper bound for d_c to be about $9.7l_\theta$. As is shown in Fig. 11(b), this estimate can be significantly reduced in the presence of azimuthal anchoring.

D. Director fluctuations at substrates near the critical point

In this section we apply the results of Sec. III B to study the correlation functions of

director fluctuations at the plates bounding the cell. Specifically, we shall use Eqs. (72)–(75) that express the correlator in terms the inverse of the matrices \hat{M}_s and \hat{M}_a given in Eqs. (59a) and (59b).

Obviously, the results obtained in the Gaussian approximation are inapplicable in the region where the structure is unstable. So, we shall restrict our considerations to the stability region and study what happen when either the thickness or q_{24} varies so as to get closer to the boundary of the instability region.

We start with the discussion of the long wavelength limit, $u \rightarrow 0$, for the matrices \hat{M}_α^{-1} . The result of calculations is that these matrices are diagonal at $u = 0$: $\hat{M}_s^{-1} = \text{diag}(w_\phi^{-1}, (w_\theta + 1)^{-1})$ and $\hat{M}_a^{-1} = \text{diag}((w_\phi + r)^{-1}, w_\theta^{-1})$. It is seen that in this limit the correlator diverges for vanishing the anchoring strengths, $W_\phi = 0$ or $W_\theta = 0$. This is a consequence of the marginal instability discussed in the preceding section.

As far as the large wavenumber (short wavelength) limit is concerned, it can be shown that in the stability region the matrices (and the correlator) both decay to zero at $u \rightarrow \infty$. Interestingly, this is not the case at the boundary of the instability interval when $q_{24} = 0$ or $q_{24} = q_c^{(2)}$. In this case we have the non-zero limits $\hat{M}_\alpha^{-1}(\infty) = (w_\theta + w_\phi)^{-1} \begin{pmatrix} 1 & \pm 1 \\ \pm 1 & 1 \end{pmatrix}$ for $q_{24} = 0$ and $q_{24} = q_c^{(2)}$, respectively. This anomaly is a precursor of the instability caused by short wavelength fluctuations. As a result, using the widespread approximation with $K_{24} = 0$ does not give the correlation functions that properly behave at large wavenumbers.

We demonstrate in Figs. 12 and 13, which show the spectra of the critical and the non-critical fluctuation modes computed from Eq. (75) at $r = 1.5$, that the critical increase of the symmetric fluctuation mode becomes sharply peaked at the critical wavenumber as the thickness of the cell approaches its critical value. In addition, Fig. 12 shows that the

symmetric and the antisymmetric modes are dominated by the in-plane and by the out-of-plane fluctuations, respectively.

V. DISCUSSION AND CONCLUSIONS

In this paper stability of the uniform director distribution in a planar NLC cell has been studied in the presence of the saddle-splay term. We have shown that the physical mechanism behind instabilities induced by the K_{24} term is governed solely by the director fluctuations at the substrates that can generally be characterized by the free energy and the probability distribution. We have developed the approach to study such instabilities by using the correlation function of the fluctuation field induced by the fluctuations at the confining wall (the surface part of the correlator) for derivation of the stability conditions.

This approach in combination with the mirror symmetry considerations has been applied to the case of NLC planar cell. It is found that there are two types of fluctuation modes, that we have called symmetric and antisymmetric modes, depending on the parity under the mirror symmetry transformation involving reflection in the middle plane of the cell.

We have devised the analytical method to analyze the stability conditions for the fluctuation modes of different symmetry. In this method the thickness of the cell and the fluctuation wavelength form the plane and the boundary of the instability region in this plane is described as a curve defined in the parametric form. It appears that no numerical calculations is required as far as qualitative analysis of stability diagrams is concerned. The analysis revealed the two different regimes for instabilities caused by the saddle-splay term depending on the value of K_{24} .

When K_{24} falls within the range between $2 \min(K_1, K_2)$ and $4K_1K_2/(K_1 + K_2)$, the

planar orientational structure loses its stability only in sufficiently thin cells and the critical thickness, d_c , together with the wavelength of the critical fluctuation mode, λ_c , determine the critical point. In this case, as is shown in Fig. 13, the spectrum of critical fluctuations at the substrates grows sharply peaked at the critical wavelength when approaching the critical point. The period of modulated structure emerging at the critical point is thus determined by the critical wavelength.

This K_{24} induced instability takes place at any elastic anisotropy parameter $r = K_2/K_1$. The sole exception is the case of elastic isotropy in which $K_1 = K_2$. In contrast with the periodic splay-twist Fréedericksz transition [39, 40, 41], where spatially modulated pattern comes into play only at sufficiently small twist-splay ratio with K_2/K_1 , the surface elasticity driven instability cannot be hindered by large elastic anisotropy, but rather, as is shown in Fig. 9, the greater elastic anisotropy the larger the critical thickness can be. The symmetry of the critical fluctuation mode, however, depends on the parameter r : the mode is antisymmetric at $r < 1$ and is symmetric in the opposite case of $r > 1$. Fig. 12 shows that the in-plane and out-of-plane fluctuations prevail depending on the symmetry of the fluctuation mode.

The azimuthal anchoring turned out to have a profound effect on both the critical thickness and the critical wavelength. The absence of the azimuthal anchoring presents the limiting case where the planar structure is marginally unstable with respect to the long wavelength fluctuations with $k_y = 0$ regardless of the K_{24} term. As a consequence, the critical wavelength λ_c increases indefinitely in the limit of weak azimuthal anchoring, $\lambda_c \rightarrow \infty$ at $W_\phi \rightarrow 0$, while the limiting value of the critical thickness can be computed exactly (see Eq. (94)) giving the upper bound for the critical thickness.

In Sec. IV C, the absolute upper bound for the critical thickness was found to be $16l_\theta$.

Fig. 9 shows that the critical thickness could have been significantly reduced in the presence of relatively small amount of the azimuthal anchoring.

Using the Cauchy relation: $K_{24} = (K_1 + K_2)/2$ [8, 11], we have found that the instability may occur at both sufficiently low and high twist-splay ratios with $r < 1/3$ and $r > 3$, respectively (see Fig. 11 and the related discussion at the end of Sec. IV C).

The corresponding condition for the periodic Fréedericksz transition requires the ratio r to be below $r_c \approx 0.303$ [40, 41] which places a slightly more stringent constraint on the value of r than the above inequality: $r < 1/3$. But, as is seen from Fig. 11(a), for small r , the critical thickness is an order of magnitude smaller than in the case of large r presented in Fig. 11(b), where d_c can be of order of several microns provided the extrapolation length l_θ varies in the range $0.1 - 1 \mu\text{m}$.

For typical nematics, the twist-splay ratio does not exceed unity, but close to the nematic-smectic- A transition the parameter r becomes anomalously large [4] leading to the K_{24} induced instability of the ground state at $r > 3$. This may result in the appearance of modulated orientational structures as suggested in Ref. [23].

When $K_{24} > 4K_1K_2/(K_1 + K_2)$ or $K_{24} < 0$, the short wavelength fluctuations with $\lambda < \lambda_\infty$ will render the planar structure unstable at any thickness of the cell. With the Cauchy relation such instability will take place when the twist-splay ratio is either less than 0.17 or greater than 5.82. In contrast with the above discussed regime, this instability though does not impose any restrictions on the film thickness, in general, cannot be unambiguously related to the periodic pattern formation. This case requires a more detailed additional study of orientational structures in the instability region where the Gaussian approximation is inapplicable.

Our concluding remark concerns the general method for separating out the contribution of director fluctuations at confining

walls to static correlation functions. We have demonstrated that this method can be used as a useful tool for studying orientational instabilities in confined liquid crystals. For this purpose, we have restricted ourselves to the case of uniaxial director fluctuations with uniformly distributed degree of ordering. But a complete treatment of fluctuations at confining surfaces is required in studies of such phenomena as electrohydrodynamical pattern formation [42], instabilities under shear flow [4, 43], wetting [44] and backflow [4]. These more general considerations involving fluctuations of spatially varying order parameter tensor coupled to the translational degrees of freedom is well beyond the scope of this paper and we will extend on this subject elsewhere.

Acknowledgments

The author thanks V.M. Pergamenschchik for useful discussions.

APPENDIX A: FREE ENERGY OF FLUCTUATIONS IN NEMATIC CELL

In this appendix we briefly comment on the derivation of the expression (40) for the free energy. We start with the second order expression for the free energy (8):

$$F_b^{(2)} = \frac{1}{2} \int_V \left[K_1 (\partial_y \phi + \partial_z \theta)^2 + K_2 (\partial_y \theta - \partial_z \phi)^2 + K_3 [(\partial_x \phi)^2 + (\partial_x \theta)^2] \right] dv, \quad (\text{A1})$$

$$F_s^{(2)} = \frac{1}{2} \int_S \left[W_\phi \phi^2 + W_\theta \theta^2 - K_{24} [\theta \partial_y \phi - \phi \partial_y \theta] \right] ds, \quad (\text{A2})$$

where we retain the director derivatives with respect to x for discussing its role later on.

Substituting the expansion (37) into Eqs. (A1) and (A2) will provide the free en-

ergy of the fluctuation harmonics in the following matrix form

$$F_{\mathbf{m}}^{(2)}/S = \left(1 - \frac{\delta_{0\mathbf{m}}}{2}\right) \int_{-d/2}^{d/2} dz \left[\partial_z \psi_{\mathbf{m}}^+ \hat{A}_1 \partial_z \psi_{\mathbf{m}} + \psi_{\mathbf{m}}^+ \hat{B}_1 \partial_z \psi_{\mathbf{m}} + \partial_z \psi_{\mathbf{m}}^+ \hat{B}_1^+ \psi_{\mathbf{m}} + \psi_{\mathbf{m}}^+ \hat{C}_1 \psi_{\mathbf{m}} \right] + \sum_{\mu=\pm 1} \psi_{\mathbf{m}}^+ \hat{D}_\mu \psi_{\mathbf{m}} \Big|_{z=\mu d/2}. \quad (\text{A3})$$

Using the transformation (39) will render all matrices in Eq. (A3) real-valued. These are given by

$$\hat{A}_1 = \begin{pmatrix} K_2 & 0 \\ 0 & K_1 \end{pmatrix}, \quad (\text{A4})$$

$$\hat{B}_1 = -k_y \begin{pmatrix} 0 & K_1 \\ K_2 & 0 \end{pmatrix}, \quad (\text{A5})$$

$$\hat{C}_1 = \begin{pmatrix} K_1 k_y^2 & 0 \\ 0 & K_2 k_y^2 \end{pmatrix} + K_3 k_x^2 \hat{I}, \quad (\text{A6})$$

$$\hat{D}_\mu = \mu k_y \begin{pmatrix} 0 & K_{24} \\ K_{24} & 0 \end{pmatrix} + \begin{pmatrix} W_\phi^{(\mu)} & 0 \\ 0 & W_\theta^{(\mu)} \end{pmatrix}, \quad (\text{A7})$$

where $W_\phi^{(\mu)}$ and $W_\theta^{(\mu)}$ are the azimuthal and the zenithal anchoring strengths at the substrate $z = \mu d/2$.

For a symmetric cell with identical substrates, we have $W_\phi^{(\pm)} = W_\phi$ and $W_\theta^{(\pm)} = W_\theta$. This is the case we deal with in this paper. But the generalized expression (A7) can be used to discuss the effects of anchoring energy asymmetry.

Another generalization is that the derivatives with respect to x have not been neglected from the very beginning and we have the term proportional to k_x^2 in the expression for the matrix (A6).

But the stabilizing magnetic field $\mathbf{H} = H \mathbf{e}_x$ likewise will change the matrix (A6): $\hat{C}_1 \rightarrow \hat{C}_1 + \chi_a H^2 \hat{I}$, where χ_a is the anisotropic part of the magnetic susceptibility. It follows

that the effects of non-vanishing wavenumbers k_x and of the stabilizing magnetic field are equivalent, so that, at $k_x \neq 0$, the structure is more stable than in the case with $k_x = 0$. Thus, the fluctuation harmonics with $k_x \neq 0$ do not affect the results of stability analysis and can be safely eliminated from the consideration.

Assuming that $k_x = 0$ and the cell is symmetric, Eqs. (A3)–(A7) can now be rewritten in terms of the dimensionless parameters defined in Eqs. (46) and (47) to yield the expressions (38)–(45).

APPENDIX B: GREEN FUNCTION METHOD FOR NEMATIC CELL

In this appendix we deduce an expression for the correlator of director fluctuations in the NLC cell by using the Green function formalism described in Sec. II B. We shall find that this method can also be employed to rederive the result for the surface part of the correlator given in Eqs. (68) and (69). In addition, this appendix provides a number of technical details omitted in the bulk of the paper.

We start with the expression for the free energy functional (41) taken, similarly to Eq. (10), in the following form

$$S_m^{(b)}[\psi] = -u \int_{-u}^u \psi^+ \hat{L} \psi \, d\tau + u \sum_{\mu=\pm 1} \psi^+ \hat{Q}_\mu^{(b)} \psi \Big|_{\tau=\mu u}, \quad (\text{B1})$$

$$\hat{Q}_\mu^{(b)} = \mu \left(\hat{A} \partial_\tau - \frac{1}{2} \hat{B} \right). \quad (\text{B2})$$

Substituting the fluctuation field (62) expressed in terms of the matrices $\hat{\Psi}^{(\pm)}$ that satisfy the Euler-Lagrange equations (48) and meet the boundary conditions (63) into Eqs. (B1) and (42) gives the matrix \hat{N} that enters Eq. (66)

$$\hat{N} = \begin{pmatrix} \hat{N}_{++} & \hat{N}_{+-} \\ \hat{N}_{-+} & \hat{N}_{--} \end{pmatrix}, \quad (\text{B3})$$

where

$$\hat{N}_{\mu\nu} = \hat{Q}_\mu \hat{\Psi}^{(\nu)} \Big|_{\tau=\mu u} = u \hat{N}_{\mu\nu}^{(b)} + \delta_{\mu\nu} \hat{Q}_\mu^{(s)}, \quad \hat{Q}_\mu = u \hat{Q}_\mu^{(b)} + \hat{Q}_\mu^{(s)}, \quad (\text{B4})$$

$$\hat{N}_{\mu\nu}^{(b)} = \hat{Q}_\mu^{(b)} \hat{\Psi}^{(\nu)} \Big|_{\tau=\mu u}. \quad (\text{B5})$$

We define the Green function as the solution of the following boundary value problem:

$$\hat{L} \hat{G}(\tau, \tau') = -\delta(\tau - \tau') \hat{I}, \quad (\text{B6a})$$

$$\hat{Q}_\pm \hat{G} \Big|_{\tau=\pm u} = 0. \quad (\text{B6b})$$

Since the operator \hat{K} from Eq. (23a) is proportional to the operator $-\hat{L}$: $\hat{K} = -uK_1S/d\hat{L}$, we need to modify the relation (22) linking the Green function and the correlator as follows

$$\hat{C}(\tau, \tau') = \frac{k_B T d}{uK_1 S} \hat{G}(\tau, \tau'). \quad (\text{B7})$$

Next we seek the Green function \hat{G} in the form of a sum

$$\hat{G}(\tau, \tau') = \hat{G}^{(b)}(\tau, \tau') + \hat{G}^{(s)}(\tau, \tau'), \quad (\text{B8})$$

where $\hat{G}^{(b)}$ is the Green function of the Dirichlet problem:

$$\hat{L} \hat{G}^{(b)}(\tau, \tau') = -\delta(\tau - \tau') \hat{I}, \quad (\text{B9a})$$

$$\hat{G}^{(b)}(\pm u, \tau') = 0. \quad (\text{B9b})$$

The boundary conditions (B9b) of the Dirichlet problem present the limiting case of strong anchoring and the Green function $\hat{G}^{(b)}$ is proportional to the bulk part of the correlator (B7).

Since the sum (B8) is the solution of the problem (B6), the equations and the boundary conditions for $\hat{G}^{(s)}$ are given by

$$\hat{L} \hat{G}^{(s)} = 0, \quad (\text{B10a})$$

$$\hat{Q}_\mu \hat{G}^{(s)} \Big|_{\tau=\mu u} = -u \hat{Q}_\mu^{(b)} \hat{G}^{(b)} \Big|_{\tau=\mu u}. \quad (\text{B10b})$$

Clearly, the surface part of the Green function represented by $\hat{G}^{(s)}$ accounts for the difference between the boundary conditions (B6b) and the strong anchoring conditions (B9b).

We have already pointed out the difference between the free energy (10) and the functional (B1) above the modified relation (B7). Likewise, this difference will slightly change the Green formula (12)

$$\begin{aligned} & \int_{-u}^u [\psi^+ \hat{L}\varphi - \varphi^+ \hat{L}\psi] d\tau \\ &= \sum_{\mu=\pm 1} \left[\psi^+ \hat{Q}_\mu^{(b)} \varphi - \varphi^+ \hat{Q}_\mu^{(b)} \psi \right]_{\tau=\mu u}. \end{aligned} \quad (\text{B11})$$

There are two important relations that almost immediately follow from the Green formula (B11):

$$-\hat{Q}_\mu^{(b)} \hat{G}^{(b)}(\tau, \tau') \Big|_{\tau=\mu u} = [\hat{\Psi}^{(\mu)}(\tau')]^+ \quad (\text{B12})$$

and

$$[\hat{N}_{\mu\nu}^{(b)}]^+ = \hat{N}_{\nu\mu}^{(b)}. \quad (\text{B13})$$

Eq. (B12) can be derived from Eq. (B11) by setting $\psi = \hat{G}^{(b)}(\tau, \tau')$ and $\varphi = \hat{\Psi}^{(\mu)}(\tau)\varphi^{(\mu)}$, whereas for the relation (B13) the substitution is: $\psi = \hat{\Psi}^{(\nu)}(\tau)\psi^{(\nu)}$ and $\varphi = \hat{\Psi}^{(\mu)}(\tau)\varphi^{(\mu)}$.

Combining Eqs. (B3)–(B5) and the relation (B13) shows that the matrix \hat{N} is symmetric

$$\hat{N}^+ = \hat{N}. \quad (\text{B14})$$

So, the matrices that enter the right hand sides of Eqs. (66) and (69) are identical. In addition, the matrices \hat{M}_α defined in Eq. (58) are also symmetric. The latter, however, can be seen from the explicit formulas (59).

Now we write the surface part of the Green function as the general solution of Eq. (B10a)

$$\hat{G}^{(s)}(\tau, \tau') = \sum_{\nu=\pm 1} \hat{\Psi}^{(\nu)}(\tau) \hat{\Theta}^{(\nu)}(\tau') \quad (\text{B15})$$

and compute the matrices $\hat{\Theta}^{(\nu)}(\tau')$ from the boundary conditions (B10b). The right hand side of Eq. (B10b) can be simplified by means of the relation (B12). Then substituting Eq. (B15) into Eq. (B10b) and using Eq. (B4) yield the equations for $\hat{\Theta}^{(\nu)}(\tau')$ in the final form

$$\sum_{\nu=\pm 1} \hat{N}_{\mu\nu} \hat{\Theta}^{(\nu)}(\tau') = u [\hat{\Psi}^{(\mu)}(\tau')]^+. \quad (\text{B16})$$

It can now be easily verified that Eqs. (B7), (B8), (B15) and (B16) provide the expression for the surface part of the correlator given in Eqs. (68) and (69).

The relation (B12) can also be applied to derive the bulk part of the Green function by means of the so-called Wronski construction [28]. The result is

$$\begin{aligned} \hat{G}^{(b)} &= \begin{cases} \hat{\Psi}^{(+)}(\tau) \hat{R} [\hat{\Psi}^{(-)}(\tau')]^+, & \tau \leq \tau' \\ \hat{\Psi}^{(-)}(\tau) \hat{R}^+ [\hat{\Psi}^{(+)}(\tau')]^+, & \tau \geq \tau' \end{cases}, \\ \hat{R} &= -[\hat{N}_{-+}]^{-1}. \end{aligned} \quad (\text{B17})$$

Our final remark concerns the symmetry relation

$$\hat{\Psi}^{(-\mu)}(\tau) = \hat{P} \hat{\Psi}^{(\mu)}(-\tau) \hat{P} \quad (\text{B18})$$

that follows from Eqs. (64a) and (64b) and in combination with Eqs. (B4) and (B5) gives the following result

$$\hat{N}_{-\mu, -\nu}^{(b)} = \hat{P} \hat{N}_{\mu\nu}^{(b)} \hat{P}, \quad (\text{B19a})$$

$$\hat{N}_{-\mu, -\nu} = \hat{P} \hat{N}_{\mu\nu} \hat{P}. \quad (\text{B19b})$$

This result simplifies algebraic verification of the relation (67).

-
- [1] J. W. Doane, in *Liquid Crystals — Application and Uses*, edited by B. Bahadur (World Scientific, Singapore, 1990), vol. 1, p. 361.
- [2] G. P. Crawford and J. W. Doane, *Modern Phys. Lett. B* **7**, 1785 (1993).
- [3] G. P. Crawford and S. Žumer, eds., *Liquid Crystals in Complex Geometries* (Taylor & Francis, London, 1996).
- [4] P. G. de Gennes and J. Prost, *The Physics of Liquid Crystals* (Clarendon Press, Oxford, 1993).
- [5] P. M. Chaikin and T. C. Lubensky, *Principles of Condensed Matter Physics* (Cambridge University Press, Cambridge, 1995).
- [6] F. C. Frank, *Discuss. Faraday Soc.* **25**, 19 (1958).
- [7] T. C. Lubensky, *Phys. Rev. A* **2**, 2497 (1970).
- [8] J. Nehring and A. Saupe, *J. Chem. Phys.* **54**, 337 (1971).
- [9] S. Faetti, *Phys. Rev. E* **49**, 4192 (1994).
- [10] V. M. Pergamenshchik and S. B. Chernyshuk, *Phys. Rev. E* **66**, 051712 (2002).
- [11] S. Faetti and M. Riccardi, *J. Phys. II France* **5**, 1165 (1995).
- [12] H. Yokoyama, *Phys. Rev. E* **55**, 2938 (1997).
- [13] V. M. Pergamenshchik and S. Žumer, *Phys. Rev. E* **58**, R2531 (1999).
- [14] D. W. Allender, G. P. Crawford, and J. W. Doane, *Phys. Rev. Lett.* **67**, 1442 (1991).
- [15] G. P. Crawford, D. W. Allender, and J. W. Doane, *Phys. Rev. A* **45**, 8693 (1992).
- [16] R. D. Polak, G. P. Crawford, B. C. Kostival, J. W. Doane, and S. Žumer, *Phys. Rev. E* **49**, R978 (1994).
- [17] V. M. Pergamenshchik, *Phys. Rev. E* **47**, 1881 (1993).
- [18] A. Sparavigna, O. D. Lavrentovich, and A. Strigazzi, *Phys. Rev. E* **49**, 1344 (1994).
- [19] O. D. Lavrentovich and V. M. Pergamenshchik, *Phys. Rev. Lett.* **73**, 979 (1994).
- [20] O. D. Lavrentovich and V. M. Pergamenshchik, *Int. J. Mod. Phys. B* **12**, 2389 (1995).
- [21] A. D. Kiselev and V. Y. Reshetnyak, *Mol. Cryst. Liq. Cryst.* **321**, 133 (1998).
- [22] V. M. Pergamenshchik, *Phys. Rev. E* **61**, 3936 (2000).
- [23] G. Barbero and V. M. Pergamenshchik, *Phys. Rev. E* **66**, 051706 (2002).
- [24] J. L. Ericksen, *Phys. Fluids* **9**, 1205 (1966).
- [25] A. L. Alexe-Ionescu, G. Barbero, and I. Lelidis, *Phys. Rev. E* **66**, 061706 (2002).
- [26] J. Zinn-Justin, *Quantum Field Theory and Critical Phenomena* (Clarendon Press, Oxford, 1993), 2nd ed.
- [27] J. Glimm and A. Jaffe, *Quantum Physics: A Functional Integral Point of View* (Springer-Verlag, NY, 1981).
- [28] H. Kleinert, *Path Integrals in Quantum Mechanics, Statistics and Polymer Physics* (Clarendon Press, Oxford, 1999).
- [29] A. N. Shalaginov and V. P. Romanov, *Phys. Rev. E* **48**, 1073 (1993).
- [30] A. Y. Val'kov, V. P. Romanov, and A. N. Shalaginov, *Sov. Phys. Usp.* **164**, 149 (1994).
- [31] S. Stallinga, M. M. Wittebrood, D. H. Luijendijk, and T. Rasing, *Phys. Rev. E* **53**, 6085 (1996).
- [32] M. M. Wittebrood, T. Rasing, S. Stallinga, and I. Mušević, *Phys. Rev. Lett.* **80**, 1232 (1998).
- [33] A. Mertelj and M. Čopič, *Phys. Rev. E* **61**, 1622 (2000).
- [34] S. A. Pikin, *Structural Transformations in Liquid Crystals* (Gordon and Breach, NY, 1991).
- [35] P. Galatola, C. Oldano, and M. Rajteri, *Phys. Rev. E* **49**, 1458 (1994).
- [36] A. D. Kiselev and V. Y. Reshetnyak, *JETP* **107**, 1552 (1995).
- [37] A. Rapini and M. Papoular, *J. Phys. (Paris) Colloq. C4* **30**, 54 (1969).
- [38] W. Zhao, C.-X. Wu, and M. Iwamoto, *Phys. Rev. E* **65**, 031709 (2002).

- [39] F. Lonberg and R. B. Meyer, Phys. Rev. Lett. **55**, 718 (1985).
- [40] W. Zimmermann and L. Kramer, Phys. Rev. Lett. **56**, 2655 (1986).
- [41] E. Miraldi, C. Oldano, and A. Strigazzi, Phys. Rev. A **34**, 4348 (1986).
- [42] A. Buka and L. Kramer, eds., *Pattern Formation in Liquid Crystals* (Springer Verlag, New York, 1996).
- [43] A. V. Alonso, A. A. Wheeler, and T. J. Sluckin, Proc. R. Soc. Lond. A **459**, 195 (2003).
- [44] P. Ziherl, A. Šarlah, and S. Žumer, Phys. Rev. E **58**, 602 (1998).